

Late Holocene volcanic stratigraphy and eruption chronology of the dacitic Young Doña Juana volcano, Colombia

Natalia Pardo^{1,†}, Roberto Sulpizio², Federico Lucchi³, Guido Giordano⁴, Shane Cronin⁵, Bernardo A. Pulgarín⁶, Matteo Roverato⁷, Ana María Correa-Tamayo⁶, Ricardo Camacho^{8,9}, and Miguel A. Cabrera⁸

¹Departamento de Geociencias, Universidad de Los Andes, Carrera 1 # 18A-12, Bogotá DC, Colombia

²Dipartimento di Scienze della Terra, Università degli Studi di Bari Aldo Moro, 70121 Bari, Italy

³Dipartimento di Scienze Biologiche, Geologiche e Ambientali, Alma Mater Studiorum, Università di Bologna, 40126 Bologna, Italy

⁴Dipartimento di Scienze, Università Roma-tre, I-00146 Rome, Italy

⁵School of Environment, The University of Auckland, Private Bag 92019, Auckland, New Zealand

⁶Servicio Geológico Colombiano, Diagonal 53 # 34-53, Bogotá, Colombia

⁷Department of Earth Science, University of Geneva, CH-1205 Geneva, Switzerland

⁸Departamento de Ingeniería Civil, Universidad de Los Andes, Carrera 1 # 18A-12, Bogotá DC, Colombia

⁹Centre for Disaster Management and Public Safety (CDMPS), Centre for Spatial Data Infrastructures and Land Administration (CSDILA), Department of Infrastructure Engineering, The University of Melbourne, Parkville, VIC 3010, Australia

ABSTRACT

We present the late Holocene eruption history of the poorly known Doña Juana volcanic complex, in SW Colombia, which last erupted in the twentieth century. This represents a case study for potentially active volcanism in the rural Northern Andes, where tropical climate conditions and a fragmented social memory blur the record of dormant volcanoes. We reconstructed the volcanic stratigraphy of the central-summit vent area by integrating new mapping at 1:5000 scale with radiocarbon ages, sedimentology analysis, and historical chronicles. Our results revealed cyclic transitions from lava-dome growth phases and collapse to explosive Vulcanian and possibly subplinian phases. Pyroclastic density currents were generated by dome collapse producing block-and-ash flows or by pyroclastic fountain/column collapse and were rapidly channeled into the deeply incised fluvial valleys around the volcano summit. The pyroclastic density currents were $\sim 4\text{--}10 \times 10^6 \text{ m}^3$ in volume and deposited under granular flow- or fluid escape-dominated depositional regimes at high clast concentrations. In places, more dilute upper portions reached a wider areal distribution that affected the inhabited areas on high depositional terraces. The coefficient of friction ($\Delta H/L$) is higher for block-and-ash

flows and dense lava-bearing fountain/low-column-collapse pyroclastic density currents compared to pumice-bearing, column-collapse pyroclastic density currents. Associated mass-wasting processes included syneruptive and interruptive debris flows, with the last one documented in 1936 CE.


INTRODUCTION

In Colombia, monitoring networks are prioritized at volcanoes showing frequent unrest or at those with written eruption records, including the first chronicles of Pedro Cieza de León or Fray Pedro Simón during the Spanish colonization in the sixteenth century. Since the Nevado del Ruiz-Armero disaster in 1985 (Voight, 1990), volcanic surveillance and short-term volcanic hazard assessment have been improved locally (Servicio Geológico Colombiano, 2022; Cortés, 2011; Driedger et al., 2020). However, knowledge gaps remain at several of the potentially active volcanoes of the Northern Andes arc showing long dormancy periods (e.g., Samaniego et al., 1998; Hidalgo et al., 2008; Robin et al., 2008, 2010; Le Pennec et al., 2011). Eruptions at these volcanic centers remain extremely hazardous, due in part to the growth of surrounding populations, especially those where conflict and migration have fragmented intergenerational social memory (Siddiqi et al., 2019; Jenkins et al., 2020; Espinosa-Arango and Prieto, 2022), and oral accounts remain unclear or untrusted (Calder et al., 1999; Miyabuchi, 1999; Macorps et al., 2018; Monteil et al., 2020).

This work focused on developing a robust geologic framework and interpreting past eruption processes at the poorly known, calc-alkaline dacitic Doña Juana volcanic complex (Pardo et al., 2019). The completeness of the geologic record here is compromised by fast rates of weathering and erosion in the tropical climate and active tectonics across the North Andean block (Gregory-Wodzicki, 2000; Montgomery et al., 2001; Mora et al., 2008). In addition, there is a fragmented oral chronology of eruptions between 1897 and 1936 CE (Espinosa, 2012), with reports of damage and casualties at Las Mesas village and surrounding farms (Fig. 1). We therefore carried out new detailed geologic mapping and lithofacies analysis of the most recent Doña Juana volcanic complex erupted products, with emphasis on pyroclastic material, combined with new ¹⁴C radiometric ages, historical chronicles, literature review, and interviews with local elders. From these data, our goals were to (1) define and characterize the late Holocene eruption history and volcano behavior of the Doña Juana volcanic complex and (2) compile a new baseline of knowledge on a potentially active volcanic center of the Northern Andes experiencing explosive activity during the twentieth century.

GEOLOGIC SETTING

The Doña Juana volcanic complex is located in the region of Nariño, SW Colombia (Figs. 1A and 1B), and it is part of the SW-NE active volcanic arc of the Northern Andes where the Nazca

Natalia Pardo  <https://orcid.org/0000-0002-8247-4116>

[†]n.pardo@uniandes.edu.co.

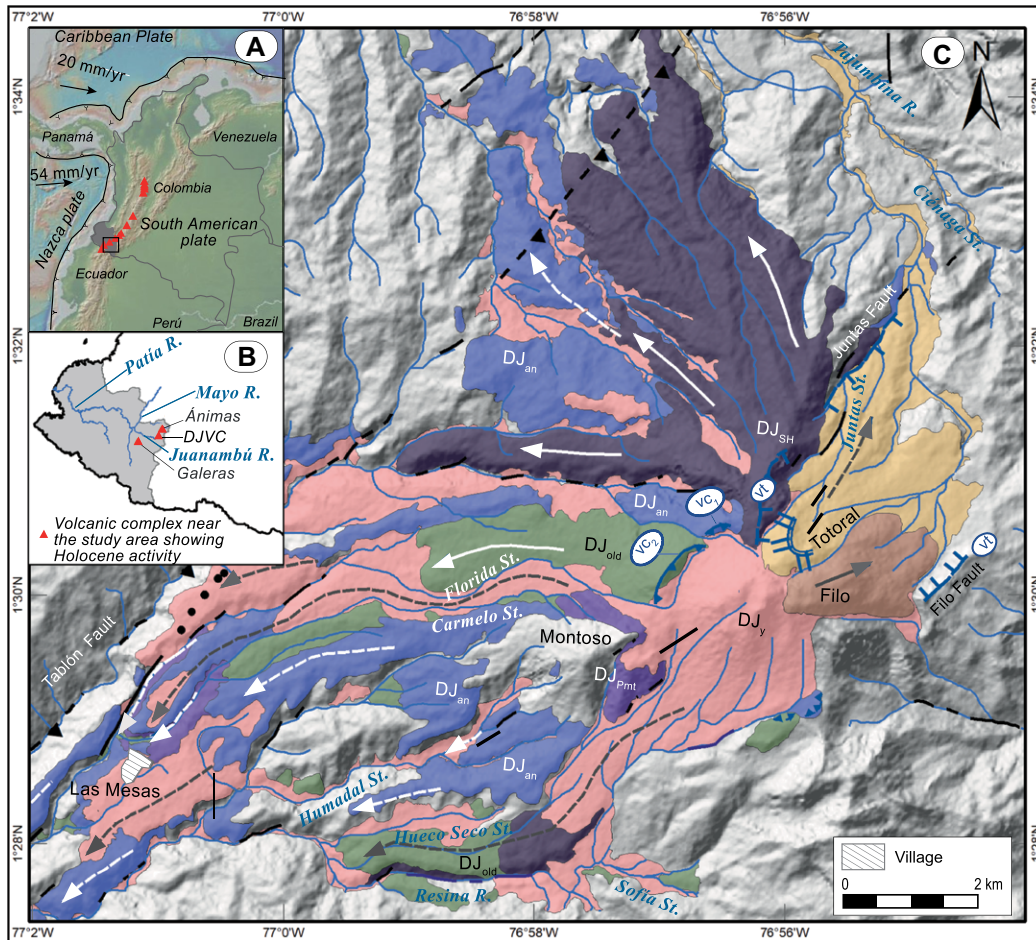


Figure 1. Simplified 1:50,000 geologic map of the Doña Juana volcanic complex (DJVC), SW Colombia (modified from Pardo et al., 2019), showing the main volcanic edifices and volcanic features, and the volcano-tectonic and structural features in the study area. R—River; St—stream.

Volcanic Edifices	Age Range	Volcano-tectonic collapse structures	Structural (Tectonic) features
Young Doña Juana	≤ 6 cal. k.y. B.P. based on ¹⁴ C data	Volcano-tectonic rim depression	Covered fault
Totoral	^{Ar} ⁴⁰ / ^{Ar} ³⁹ : ~231–77 ka	Non-explosive collapse caldera rim	Main regional fault
Filo	^{Ar} ⁴⁰ / ^{Ar} ³⁹ : ~878–312 ka	Chronological order of non-explosive collapse calderas	Lineament trace
Old Doña Juana	~1125–1097 ka		Volcanic features
Ancestral Doña Juana			Lava flow direction
Pre-Montoso			Volcaniclastic product flow direction
Santa Helena			Partially collapsed lava dome
Basement			

plate subducts beneath South America (Taboada et al., 2000; Cortés and Angelier, 2005). Similar to most active volcanoes in the Central Cordillera of Colombia (Monsalve-Bustamante, 2020), the oldest units (lava flows) known at the Doña Juana volcanic complex unconformably overlie a polymetamorphic Cretaceous basement (Cediél et al., 2003) and date to the Pleistocene.

The geologic setting presented here refers to Pardo et al. (2019). The volcanic complex consists of three spatially overlapping and successively active volcanoes: Santa Helena (ca. 1125–1097 ka), Ancestral Doña Juana (ca. 878–312 ka), and Old Doña Juana (ca. 231–77 ka). The summit of each edifice is truncated by

a narrow extensional structure (vt) bordered by regional NE-SW faults, where volcanism was concentrated, together with two nested, tectonically controlled, collapse calderas (vc₁ and vc₂, respectively) and lateral volcanic collapses (Fig. 1C).

The Holocene stratigraphic record of Doña Juana volcanic complex relates to three summit vent areas: (1) Young Doña Juana (central summit), (2) Totoral (NE), and (3) Phyllo (E), which include lava domes emplaced within and along the borders of the youngest vc₂ caldera (Fig. 1C). The corresponding eruptive products overlie a prominent regional marker bed, a Plinian pumice-fall deposit sourced from the

adjacent Las Ánimas volcano (Fig. 1B). The fall deposit has a maximum age of 5904 ± 30 ¹⁴C yr B.P. (6794–6661 calibrated yr B.P.) and a minimum age of 4422 ± 28–4250 ± 30 ¹⁴C yr B.P. (5056–4813 cal. yr B.P.). The Totoral and Phyllo vents (Fig. 1B) were mainly effusive. Block-and-ash flows and reworked volcaniclastic deposits related to the collapse of earlier Totoral lava domes are the only recent Doña Juana volcanic complex products to the northeast of the study area (Ciénaga formation; Pardo et al., 2019). Young Doña Juana is the main active vent, which experienced explosive and effusive activity along with recurrent generation of pyroclastic density currents and

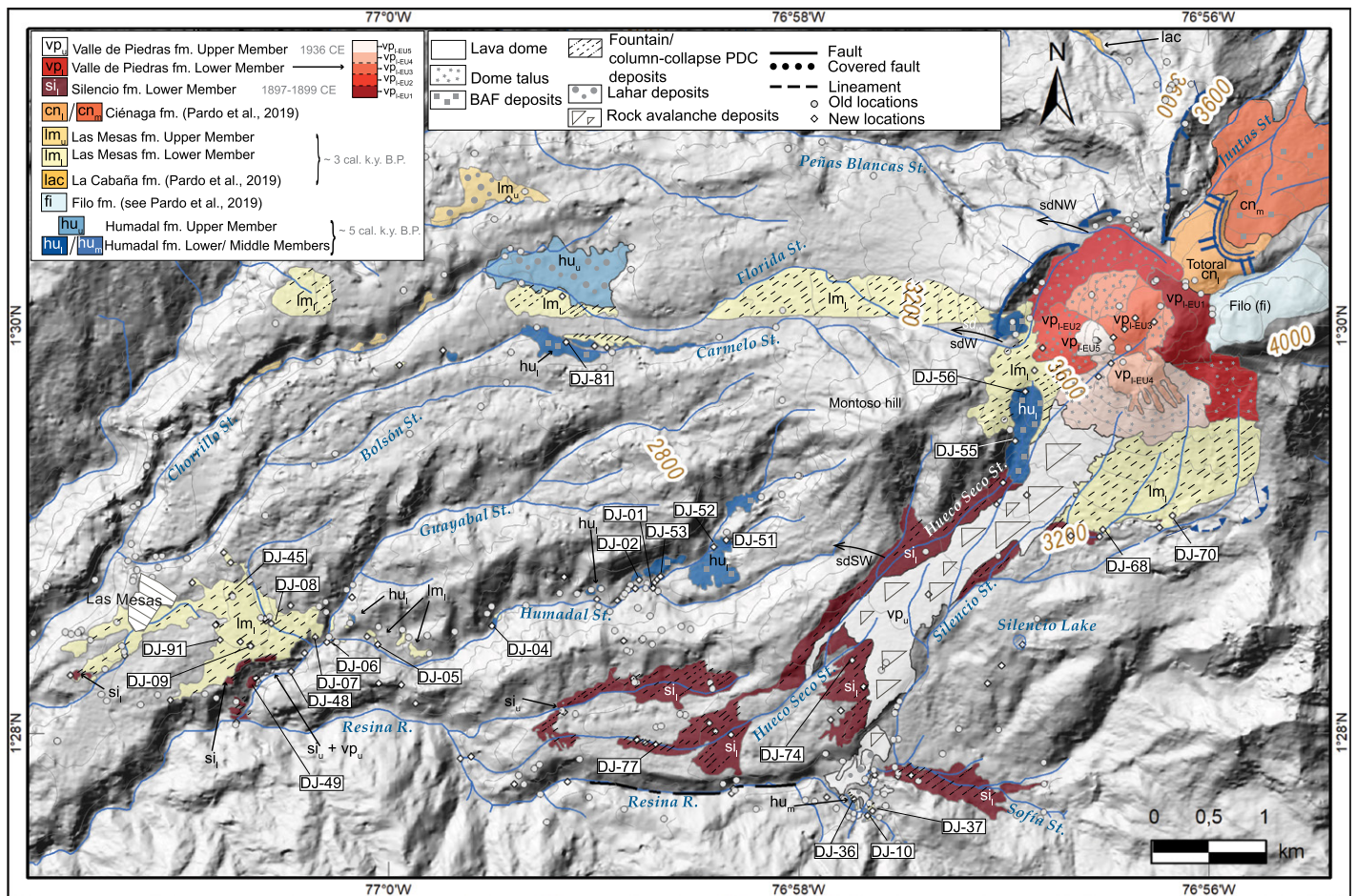


Figure 2. New geologic map of the late Holocene products in the study area relevant to the Young Doña Juana, Totoral, and Phyllo summit vent regions. Arrows marked as sdN, sdW, and sdSW are saddles that favored pyroclastic density current outflows from the vc_2 caldera. St.—stream; R.—River; BAF—block-and-ash flow; PDC—pyroclastic density current. The conventions for volcano-tectonic structures are the same as shown in Figure 1.

lahars. Juvenile products are seriate porphyritic dacites of variable color and vesicularity, but with a homogeneous whole-rock composition ($62.36 < SiO_2 \text{ wt\%} < 66.61$, anhydrous base) and mineral association of plagioclase + amphibole + quartz + biotite + oxides_{Fe-Ti} ± pyroxene ± apatite.

METHODS

We focused on the geology of the Young Doña Juana central summit vent zone because it is the best exposed feature, it is the only one showing pyroclastic (in addition to effusive) activity, and it has affected the inhabited territory to the west of the volcano in the twentieth century. We described new outcrops at 93 locations in the upper basin of the Juanambú River, with particular detail in the area of the Las Mesas village located on a depositional terrace beside the Humadal and Resina fluvial valleys (Figs. 1 and 2; labeled as DJ- in Supplemental Material

Supplemental Material 1¹). We used a 5-m-resolution digital elevation model (DEM) obtained from 2007 GeoSAR images 1473, 1474, and 1574 of the Colombian National Image Bank (<https://igac.gov.co/es/noticias/banco-nacional-de-imagenes-colombia-vista-desde-el-espacio>) to construct a shaded relief map and a slope map, and the geologic information was recorded in ArcMap (v. 10.7; ©ESRI, 2019) at a scale of 1:5000 (Fig. 2; Supplemental Material 1).

¹Supplemental Material. Supplemental Material 1: Link to the interactive map (1.1), histograms (1.2), and statistics (1.3) of grain-size distributions of each pyroclastic unit. Supplemental Material 2: Radiocarbon dating ($n = 90$) and whole-rock geochemical data ($n = 27$) of juvenile clasts. Supplemental Material 3: Details on volume calculation and calculation of main geometric parameters following Giordano and Cas (2021). Please visit <https://doi.org/10.1130/GSAB.S.21365685> to access the supplemental material and contact editing@geosociety.org with any questions.

We distinguished lithostratigraphic units (formations) according to distinctive lithologic features and stratigraphic positions, corroborated by radiocarbon ages (Supplemental Material 2). Formations were subdivided into members characterized by distinct lithology and lithofacies associations (Table 1). Members discriminate lava domes, pyroclastic products, and reworked volcanoclastic deposits (hereafter volcanoclastics). The pyroclastic members were subdivided into eruption units, each one representing the deposit of an individual and continuous eruption delimited by significant time breaks (Fisher and Schmincke, 1984). These eruption units are characterized by distinctive lithofacies associations and are separated by erosion surfaces, paleosols, and/or detrital deposits suggesting significant volcanic quiescence of variable duration (Lucchi, 2013). Hence, a particular pyroclastic member consists of one or multiple eruption units (in which case, they show overlapping radiocarbon ages) and represents the total

TABLE 1. DEFINITION OF LITHOFACIES CODES AND LITHOFACIES ASSOCIATIONS FOR STUDIED UNITS AND THEIR INTERPRETATION: PYROCLASTIC DEPOSIT LITHOFACIES*

Lithofacies codes	Description	Interpretation	Unit	Ref. Fig.
TABLE 1A Massive lithofacies mA, maaccrA	Massive ash (mA). Thicknesses range within a few centimeters, variable at outcrop scale. Moderately to well sorted. These massive ash lithofacies may contain ash aggregates (maaccrA). Also, there are discontinuous ash patches of pumice and/or lithic coarse massive ash within the soils.	Gentle settling from a slow-moving, ground-hugging ash cloud. In some cases, fine ash is elutriated from the basal part of pyroclastic density currents (PDCs). They may occur in overbank environments as result of rapid deposition from a fluid escape-dominated flow-boundary zone. Where clast-supported coarse ash, fallout deposition is inferred.	Im_{1-EU1}, Im_{1-EU2} Si_{1-EU1}, Si_{1-EU2}	6C–6D
mAL, mALB, mB _(rp) , mBLA, mBLA _(rp) , mALB _(rp) , mAL _(rp) , mB _(rp) , mLA _(rp) , mALB _(rp) , mBLA _(rp) , mALB _(g-c) , mALB _(g-c)	Massive ash and lapilli (mAL), massive ash and lapilli with abundant blocks (mALB), massive blocks with minor lapilli and ash (mBLA), sometimes with reverse grading of lithic clasts (mBLA[rl], mALB[rl], mAL[rl]). Beside reverse grading, larger blocks may show jigsaw structures (mB[jw]LA[rl]). Reverse grading of pumice (mALB[rp]) or coarse-tail grading (mBLA[g-ct], mALB[g-ct]) may occur locally. The former form levées in proximal areas, where they are rich in bread-crust pumice bombs. They are generally poorly to moderately sorted deposits, forming terraces and ranging in thickness from a few meters to decimeters. Where monolithologic and dominated by block-size dense dacite clasts (mB _p), deposits are valley confined, and they may form levées or show a hummocky morphology on the landscape. Megablocks may occur on top and in front of the steep terminations of hummocks. The thickest exposures are predominant at marked breaks in slope on steep surfaces. Where ash and lapilli dominate over blocks, the latter may show cooling joints, and tabular clasts form flat-lying trains parallel to base and are crudely imbricated. Where slightly more heterolithologic (including vesicular clasts) and matrix rich, bread-crust and cauliflower bombs may occur at proximal sites, and clasts are embedded in a lithic-crystalline coarse ash matrix with abundant charred tree trunks. Where thicker, a few small gas pipes are present, and the deposits are pinkish-tanned at top.	Rapid deposition from granular flow or fluid escape-dominated flow-boundary zone. Lithofacies with reversely graded blocks indicate granular flow-dominated flow-boundary zone, in which kinetic sieving and kinematic squeezing promoted the migration of larger clasts to the top. Matrix-rich lithofacies indicate a fluid escape-dominated flow-boundary zone. The lithofacies showing reverse grading of pumice and coarse-tail grading reflect the strong density segregation within the highly particle concentrated PDCs.	$hu_{1p}, hu_{1m}, Im_{1-EU1}, Im_{1-EU2}, Im_{1-EU3}, Si_{1-EU1}, Si_{1-EU2}, VP_{1p}$	5A, C 5E–5F 6A–6E 7B–7D
Lenticular lithofacies mL	Discontinuous massive deposits of locally graded lapilli. Clast-supported. Clasts are angular, and pumice clasts may show normal or reverse grading. Good to moderate sorting.	Remnants of pyroclastic fall deposits. Grading reflects changes in column height with time. These lenses indicate simultaneous deposition from PDCs and fallout from the umbrella cloud of sustained columns. Alternatively, these form by traction at the PDC boundary zone.	$Si_{1-EU3}, Si_{1-EU4}, Im_{1-EU1}, -4$	5D
lensL	Lenses of lapilli (lensL). Individual lenses are massive and poorly sorted, and most clasts are subangular. The thickness of individual lenses ranges within a few centimeters, and lenses are enclosed within mLA, mALB, or mAL lithofacies. In other cases, such lenses are found as individual units or within soil profiles. Good sorting.	Deposition from a flow-boundary zone dominated by traction processes supported by fluid turbulence.	hu_{1p}	
Stratified lithofacies sLA	Stratified lapilli and ash. Parallel to low-angle cross-stratified beds. The stratification is given by grain size and color contrast between poorly sorted, orange-stained, lapilli-dominated beds and gray, massive to weakly and discontinuous low-angle cross-laminated ash and lapilli beds. Thicknesses of individual beds range from a few centimeters to nearly 20 cm, forming bedsets of 50–70 cm separating thicker deposits of massive lithofacies. Medium to good sorting.	Grain-by-grain deposition from a traction-dominated flow-boundary zone.	Im_{1-EU1}, Im_{1-EU2}	6C–6D
IA, w/A, wx/A	Laminated (IA) to weakly laminated (w/A) and low-angle cross-laminated ash (wx/A). Thicknesses range within a few centimeters, variable at outcrop scale. Good sorting; individual grains range from subangular to rounded. Componentry may be lithic-crystalline or vitric-crystalline. Weakly equals “diffusely” in Sulpizio and Dellino (2008).	Grain-by-grain deposition from a traction-dominated flow-boundary zone.	Im_{1-EU1}, Im_{1-EU3}	6D
xsA, xsAL, xsLA	Low-angle cross-stratified deposits of ash (xsA), ash and lapilli (xsAL), or lapilli and ash (xsLA). Dune-bedded deposits varying in thickness within a few tens of centimeters. Fine lapilli are locally aligned and are predominantly dense to poorly vesicular, medium and light gray porphyritic dacites. Medium sorting.	Rapid deposition from debris flows. Reverse grading indicates granular flow regime at time of deposition, whereas imbrication and clast-supported lenses suggest transitions towards hyperconcentrated flows. Deposition from mudflows reworking tree trunks indicate oxidation of the exposed surfaces. EpheMERAL lake deposit (temporary river damming?).	$hu_{1p}, Im_{1p}, si_{1p}, VP_{1p}$ hu_{1p}, si_{1p} si_{1p}	8B
TABLE 1B Lithofacies of secondary volcanoclastic deposits mGSM, mGSM _(rg) , mSGM, mG	Massive (mGSM) or locally reversely graded deposits of sandy muddy gravels (mGSM _(rg)), massive gravely muddy sand (mSGM), and massive gravels (mG). Very poorly sorted deposits, formed by heterolithologic gravels of variable roundness set in a sandy matrix with variable mud content. Where matrix-supported, the matrix is hardened. Weak stratification is given by multiple overlying beds showing reverse grading. Over distance, gravels show imbrication and are concentrated in lenses.			
mMSG, mSM	Massive gravely sandy mud (mMSG) or massive muddy sand (mSM). These deposits are found on flat landscapes or on hummocky landscapes located at breaks in slopes. Deposits are poorly sorted, some containing abundant large, black, unburned tree trunks. Grains are subangular to subrounded and heterolithologic, embedded in a clay-rich matrix.			
altSC	Alternating silt and clay (altSC). Local patchy deposit of thinly alternating pale gray to pinkish brown layers of well-sorted silt and clay beds.			

*Following Sulpizio et al. (2007), Sulpizio and Dellino (2008), and Sulpizio et al. (2014).

of deposits produced over an “eruption episode” (modifying Jenkins et al., 2007).

Compared to older lithostratigraphic units of Doña Juana volcanic complex (Pardo et al., 2019), the late Holocene deposits do not generally form terraces at different elevations, hindering an obvious distinction between older (higher) and younger (lower) units in a geologic setting characterized by regional uplift. The different units are commonly juxtaposed laterally against each other at heights depending on the level of accumulation within the river valleys, and they have similar lithology. This makes it difficult to unequivocally distinguish the different lithostratigraphic units (and eruption units). Therefore, our new systematic ^{14}C age data set in charred wood (Supplemental Material 2) was a major tool to develop the stratigraphic correlations. We combined 16 new radiocarbon ages and 74 previously published radiocarbon ages reported in Pardo et al. (2019). We used OxCal v4.4 (Bronk-Ramsey, 2009) for calibration by using the IntCal20 curve (Reimer et al., 2020), which is the updated calibration curve for Northern Hemisphere latitudes, and B.P. indicates the year before 1950 CE. Whole-rock compositions (6 new and 21 published) are also included in Supplemental Material 2. We attempted to correlate the geologic data from the latest eruption episode to the descriptions found in historical chronicles (Küch, 1892; Pereira-Gamba, 1919; Espinosa, 2012), local unpublished essays (Gómez-Bolaños, 2012), national newspapers (i.e., *El Espectador*, 1887; *El Heraldo*, 1899; *El Derecho*, 1936a–f; *El Tiempo*, 1936), and interviews with elders (Pulgarín et al., 2015; Arnulfo Bravo 2015, María Mercedes Muñoz 2015, Delfina Muñoz 2015, 2017, personal communications).

The main geometric parameters of deposits (outflow area, bulk volume, average thickness, equivalent runout, equivalent diameter, aspect ratio) related to pyroclastic density currents were calculated according to Giordano and Cas (2021) (see Supplemental Material 3). The interpretation of lithofacies associations for each unit (Table 1) followed classifications of Sulpizio et al. (2007, 2014) and Sulpizio and Dellino (2008).

Grain-size distributions were retrieved from field photographs and bulk samples. Coarse sizes (larger than -6ϕ) were obtained from image analysis within a 1 m by 1 m grid, using Image-J. Bulk samples were dry-sieved at 0.5ϕ fractions at the Geosciences Department laboratories of the University of Los Andes (Colombia), and particles smaller than 3ϕ were analyzed with a CILAS-1190 laser particle size analyzer at the Mechanical Engineering Department laboratories (22 °C and 50% relative humidity) of the

same university. Grain-size data were processed with GRADISTAT (Blott and Pye, 2001). We report merged histograms, but for deposits having particles coarser than -6ϕ , we discriminated the cumulative curves obtained by each method. We excluded particles coarser than -6ϕ from the data set used to calculate the F1 (wt% finer than 4ϕ) and F2 (wt% finer than 0ϕ) parameters following Walker (1983), in order to facilitate comparison between samples (Supplemental Material 1).

RESULTS

Our new 1:5000 geologic mapping (Fig. 2; see specific sampling locations in Supplemental Material 1.1), volcanic stratigraphic analysis, and sedimentologic analysis (Fig. 3) allowed us to define four formations, namely (from eldest to youngest), Humadal, Las Mesas, Silencio, and Valle de Piedras. These are mainly exposed on fluvial terraces confined to the west and southwest quadrants of the volcano summit, within the upper Juanambú River catchment (Figs. 1 and 2). The areal distribution (Fig. 2), stratigraphy (Figs. 3 and 4), and lithofacies associations (Table 1) of newly defined lithostratigraphic units and their internal subdivisions are described below.

Humadal Formation

This is the oldest late Holocene lithostratigraphic unit newly defined here for the Young Doña Juana summit vent, comprising two pyroclastic members (lower and middle) and one volcanoclastic member (upper). Contacts between the lower and middle pyroclastic members are not clearly visible in the field, and they are distinguished by different areal distributions and lithofacies associations (Figs. 2–5). Juvenile components range $62.91 < \text{SiO}_2 \text{ wt\%} < 65.71$.

Lower Member (hu_l)

This member consists of distinctively valley-confined, massive, monolithologic, poorly sorted tuff breccias showing polymodal grain-size distributions, with red and dense dacitic blocks embedded in a lithic to lithic-crystalline medium lapilli to coarse ash matrix (Supplemental Material 1). Proximal exposures occur at the base of the western flank of the Young Doña Juana summit lava domes and form depositional terraces along the Hueco Seco stream, in the northwestern sector of the vc_2 caldera (Fig. 2). They are ~ 75 -m-thick deposits of massive blocks, lapilli, and ash (lithofacies mBLA; Table 1A) surmounting the remnants of older volcanic edifices. Grain-size distributions are mesokurtic and vary from positive skewed (i.e., positive skew-

ness; location DJ-56; Blott and Pye, 2001) to symmetrical (DJ-55). Abutting the western flank of Montoso basement relief (Fig. 2; at DJ-52), the hu_l member is an ~ 15 -m-thick succession of weakly reversely graded, very thick beds hosting meter-sized jigsaw-fit blocks (lithofacies $mB_{[jw]}LA_{[r]}$; Table 1A; Figs. 5A–5C). The best exposures of hu_l occur along the Humadal stream valley (Fig. 2), on the scarp of terraces. There, this unit is 8–10 m thick and exhibits a succession of weakly reversely graded, very thick beds marked by flat-lying trains of crudely imbricated blocks that are parallel to the base (lithofacies $mBLA_{[r]}$, $mALB_{[r]}$; Table 1A; Fig. 5B). Grain-size distributions are platykurtic and range from very finely to positive skewed. Locally, the uppermost ~ 50 – 100 -cm-thick bed at such terraces is massive and distinctively matrix rich, showing ash, lapilli, and a few blocks (lithofacies $mALB$; Table 1A). The abrupt distal limit of the deposit along the Humadal stream occurs ~ 7.5 km from the Young Doña Juana summit.

Up to 10-m-thick exposures of the hu_l member occur in the headwaters of the Florida and Carmelo stream valleys to the west-northwest of the summit vent (Fig. 2). Along the Carmelo stream valley, three to four 2–3-m-thick, poorly sorted, monolithologic beds are distinguished by local concentrations of blocks at the top of each bed (lithofacies $mALB_{[r]}$; Table 1A) or by intervals of ~ 50 – 70 -cm-thick, low-angle, cross-stratified lapilli and ash (lithofacies sLA ; Table 1A; Fig. 5D) between them. The thickest, coarse-grained beds show polymodal, symmetrical, and mesokurtic grain-size distributions (at DJ-81). Rare charred wood fragments are found in this sector, providing a new radiocarbon age of 4389 ± 22 ^{14}C yr B.P. (4986–4867 cal. yr B.P.). In general, the mesokurtic to platykurtic grain-size distributions of the matrix show $-2.3 < D_{50}(\phi) < 0.03$, coarse ash contents between 26 and 55 vol%, and fine ash contents between 4 and 16 vol%.

Middle Member (hu_m)

The hu_m member is composed of gray pyroclastic deposits exposed along the southwestern flank of Young Doña Juana (Fig. 4A). These deposits fill the vc_2 caldera and form the base of a depositional terrace near the Sofia stream outflow into the Resina River, ~ 5.0 km from the current volcano summit (Fig. 2). Proximal deposits (DJ-70 in Supplemental Material 1.1; Fig. 5E) are poorly sorted, massive to weakly reversely graded tuff breccias hosting blocks, lapilli, and ash (lithofacies $mBLA_{[r]}$; Fig. 5E; Table 1A). The most complete exposures of hu_m (at DJ-10; DJ-36) are valley-confined, > 15 -m-thick, poorly sorted, massive deposits of coarse ash, lapilli, and blocks

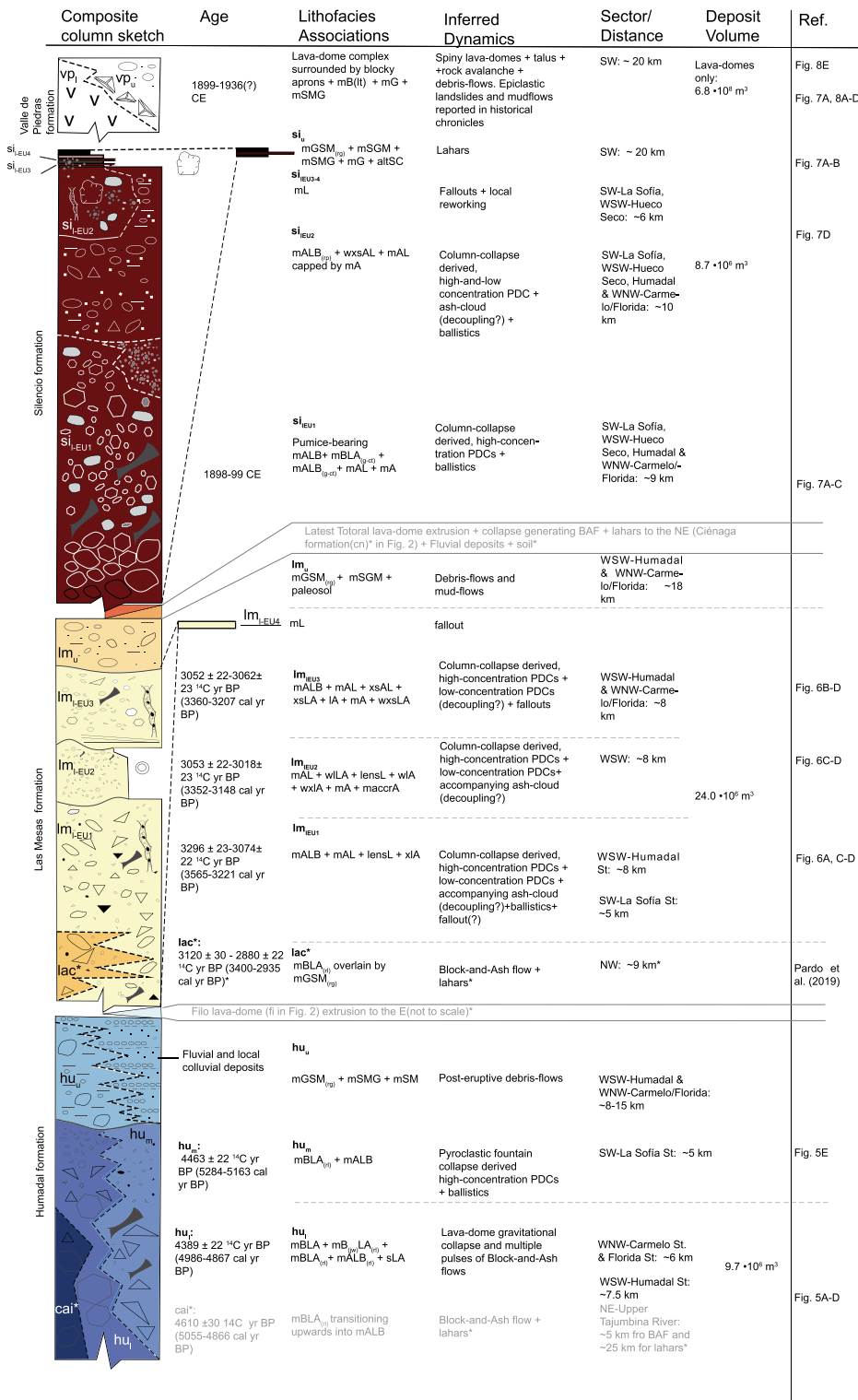


Figure 3. Composite stratigraphic column of the Young Doña Juana products relative to the late Holocene. Lithofacies associations are defined in Table 1, and spatial distribution details can be found in the text. *Described and mapped in Pardo et al. (2019) outside the study area: cai* stands for Caicuanes formation (to the NE and coeval with the Humadal formation), and lac* stands for La Cabaña formation (to the NNE and coeval with the Las Mesas formation). BAF—block-and-ash flow; PDC—pyroclastic density current.

(lithofacies mALB in Table 1A; Fig. 5F). Grain-size distributions are bimodal to polymodal, positive skewed to symmetrical, varying from mesokurtic at the base to platykurtic at the top (Supplemental Material 1.2). The matrix grain-size distributions show $D_{50}(\varphi) = -0.77$, coarse ash contents between 33 and 46 vol%, and fine ash contents between 2 and 11 vol%. Angular clasts are embedded in a lithic-crystalline matrix ranging between fine lapilli and coarse ash, with common charred wood fragments. Some bread-crust and cauliflower bombs are present. Besides the predominant dense components of porphyritic dacite, a few pale gray and brown pumiceous clasts occur. Also, oxidized schist and rounded hydrothermally altered lithics are found in the coarse lapilli to coarse ash fractions. In this study, we obtained an age of 4463 ± 22 ¹⁴C yr B.P. (5284–4976 cal. yr B.P.) in charred tree trunks. In addition, the lithofacies associations of the hu_u member of Humadal formation are similar to the coeval 4400 ± 30 ¹⁴C yr B.P. (5053–4863 cal. yr B.P.) Caicuanes formation (Fig. 3) reported by Pardo et al. (2019) outside the study area, sourced from the NE Totoral vent zone (Fig. 2).

Upper Member (hu_u)

The hu_u member overlies with sharp contact the hu_u member, or it forms low terraces juxtaposed with the hu_u member at lower elevations along the valleys of the Humadal, Carmelo, and Florida streams down to ~8–15 km from the source. The hu_u member consists of ~4–5-m-thick beds of massive to weakly reversely graded volcanoclastic deposits of very poorly sorted to poorly sorted, heterolithic (red >> gray dacites > accidental lithics) sandy-muddy gravels (lithofacies mGSM_(m); Table 1B). Gravels show variable roundness and are locally imbricated within a hardened and porous silty-clay-rich matrix. Locally, the hu_u member includes massive muddy-gravelly sands (lithofacies mSMG; Table 1B) and muddy sands (lithofacies mSM; Table 1B) containing abundant large, oxidized but uncharred tree trunks within a clay-rich matrix. These clay-rich deposits are found on high-gradient surfaces in transitional contact above the hu_u member at the western foot of the Montoso basement relief.

Las Mesas Formation

This unit is recognized along the southwestern and western flanks of Young Doña Juana, partially overlapping with the Phyllo lava dome (Fig. 2), where a whitish to pinkish hydrothermally altered zone is visible and inhabitants

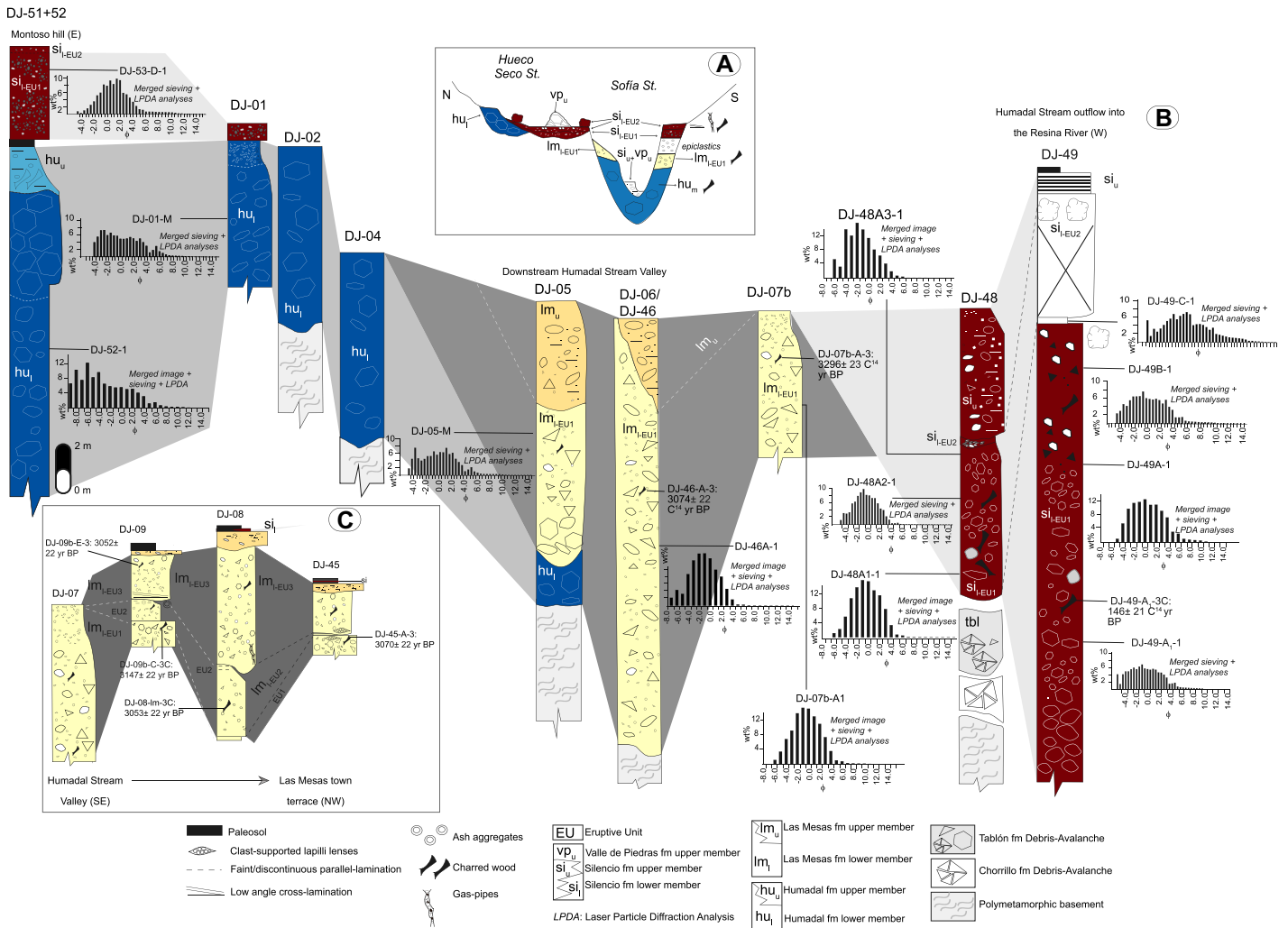


Figure 4. Cross sections constructed along the western slopes of Doña Juana volcanic complex (see location sites in the Supplemental Material 1.1 [text footnote 1]). (A) Profile across the Hueco Seco and Sofía streams shown as A-A' in Figure 1. (B) Stratigraphic column along Humadal stream. (C) Stratigraphic column from Humadal Stream up and across the terrace currently occupied by Las Mesas village. See Figure 2 for further references. The Chorrillo and Tablón formations correspond to Pleistocene debris avalanche deposits derived from sector collapses of the Santa Helena–pre-Montoso and Ancestral Doña Juana edifices, respectively (Pardo et al., 2019), and represent in many places the substratum above which the late Holocene products of Doña Juana volcanic complex were emplaced. Lithofacies associations and units are defined in Table 1 and Figure 3.

report preexisting fumaroles. The Las Mesas formation fills the vc₂ caldera and forms depositional terraces along the valleys, overlying or partially juxtaposed alongside the Humadal formation (Figs. 2 and 3). The Las Mesas formation is subdivided into a pyroclastic lower member (Im_l) and a volcanoclastic upper member (Im_u; Fig. 4).

Lower Member (Im_l)

This is a pyroclastic succession that is subdivided into four eruption units (Im_l EU1–EU4) by distinctive lithofacies associations, erosive surfaces, sharp grain-size variations, and differences in color (Figs. 3 and 6). Juvenile

clast composition is narrow ($62.36 < \text{SiO}_2 \text{ wt\%} < 66.61$).

Eruption unit Im_l EU1. Unit Im_l-EU1 forms terrace remnants along the Sofía, Humadal, Carmelo, and Florida stream valleys and interfluvies (Fig. 2). This unit is 15–20 m thick, and it consists of massive, poorly sorted ash and lapilli ± blocks (angular to subangular) embedded in a lithic-crystalline very coarse ash matrix (lithofacies mALB, mAL; Table 1A), locally showing gas pipes and containing abundant charred wood fragments. Dense to poorly vesicular medium gray > red > pale gray (porphyritic) dacites, and brown pumiceous clasts are predominant as juveniles, with

fewer hydrothermally altered and oxidized lithics, as well as metasedimentary accidental lithics (Figs. 6A–6D). At Las Mesas village, unit Im_l-EU1 overlaps with higher Pleistocene depositional terraces and is subdivided into two 15–50-cm-thick, well-sorted massive ash and lapilli beds (lithofacies mAL; Table 1A), locally embedding clast-supported lenses of fine lapilli (lithofacies lensL; Table 1A). The two beds are separated by a 5–7-cm-thick, discontinuous, fining-upward coarse to fine ash showing low-angle cross-lamination (lithofacies xlA; Table 1A). Grain-size distributions in massive lithofacies are mostly symmetrical and mesokurtic for 8.5 km downstream (Supplemental Materials 1.2

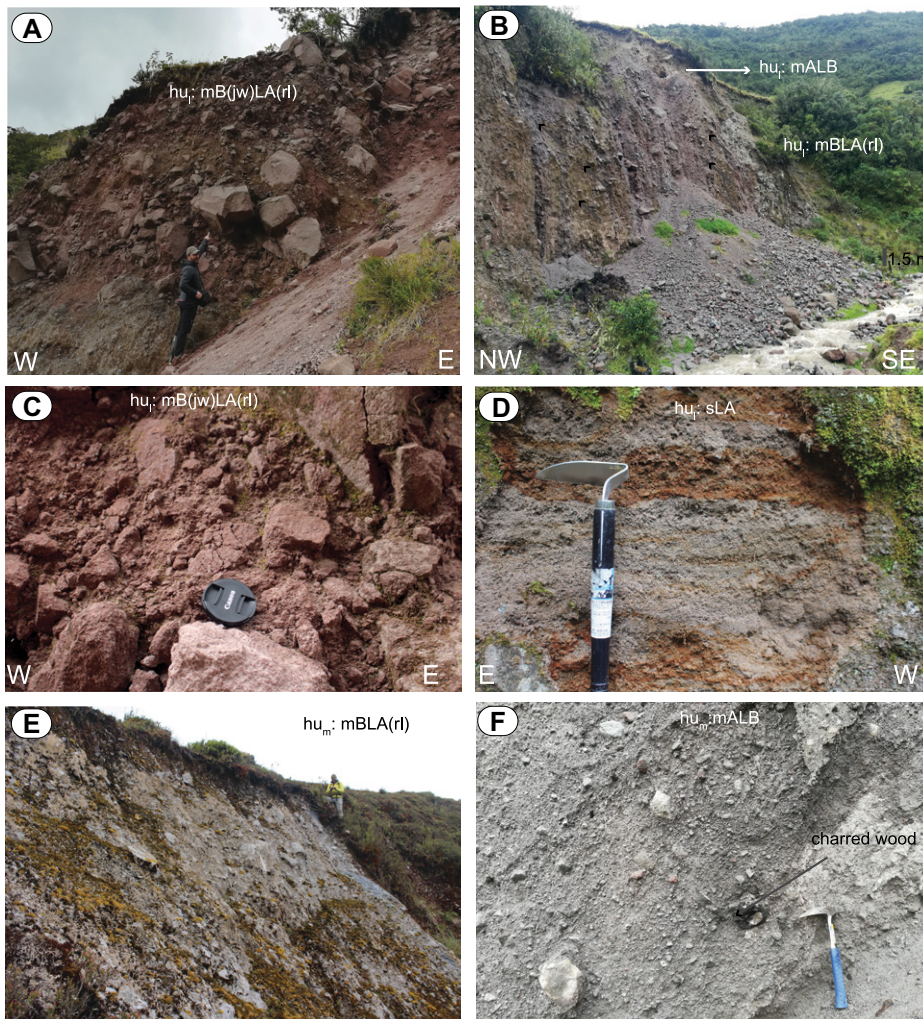


Figure 5. (A–D) Typical exposures of the lower member (hu_1) of Humadal formation at the upper Humadal Stream localities (DJ-1–5 in Supplemental Material 1.1 [see text footnote 1]), formed by block-and-ash flow deposits, and their lithofacies. (E) Depositional fan and river incision leaving terraces at the outflow of Sofia stream into the Resina River, exposing an outcrop of the middle member (hu_m) of Humadal formation. (F) Close-up of the middle member (hu_m) of Humadal formation at the outflow of the Sofia stream into the Resina River valley (DJ-10 in Supplemental Material 1.1 [see text footnote 1]) with charred wood fragments. Lithofacies codes are described in Table 1.

and 1.3). Rare positive skewed and platykurtic distributions occur where unit lm_1 -EU1 overlaps with the higher Pleistocene terraces (DJ-07), and within the lowermost massive bed found at the most distal location on top of such terraces (DJ-91). New radiocarbon ages for lm_1 -EU1 from different locations constrain its range between 3296 ± 23 yr B.P. (3565–3460 cal. yr B.P.) and 3070 ± 22 yr B.P. (3360–3217 cal. yr B.P.).

Eruption unit lm_1 -EU2. Unit lm_1 -EU2 is recognized only near the Las Mesas village, overlapping unit lm_1 -EU1 with a flat or irregular sharp contact (Figs. 6C–6D). Unit lm_1 -EU2 is a distinctively reddish brown, pinching-and-swelling, massive lapilli tuff composed of medium to

fine ash and lapilli (lithofacies mAL; Table 1A). Thickness varies laterally from 2 m to 0.01 m on an outcrop scale (Figs. 6C–6D). Thickest exposures are poorly sorted deposits showing a few gray and red dense porphyritic medium to coarse lapilli within a lithic-crystalline coarse to very fine ash containing small (<3 cm) charcoal fragments. Very rare rounded pumice lapilli and subangular metamorphic lithics also occur. Grain-size distributions obtained from the lm_1 -EU2 matrix are coarse skewed and vary from leptokurtic to mesokurtic, with coarse ash contents between 45 and 94 vol% and fine ash contents between 2 and 54 vol% (Supplemental Material 1.3). The uppermost parts of these

deposits are poorly sorted, weakly laminated fine lapilli and ash tuffs (lithofacies wLA; Table 1A) with positive skewed and leptokurtic grain-size distributions, locally containing clast-supported fine lapilli lenses (lithofacies lensL; Table 1A). At the top, these deposits are capped by a few centimeters of weakly laminated to cross-laminated, poorly sorted, very fine ash showing symmetrical and leptokurtic grain-size distributions (lithofacies wLA, wxLA; Table 1A). Laterally, these uppermost layers pass to well-sorted and massive, very coarse ash (lithofacies mA; Table 1A) exhibiting positive skewed and platykurtic grain-size distributions, locally containing ash aggregates (lithofacies maccrA; Table 1A). Small charcoal fragments found within the thickest massive lithofacies of lm_1 -EU2 were dated in this study at 3062 ± 23 ^{14}C yr B.P. (3360–3210 cal. yr B.P.) and 3053 ± 22 ^{14}C yr B.P. (3352–3208 cal. yr B.P.).

Eruption unit lm_1 -EU3. Unit lm_1 -EU3 overlaps with lm_1 -EU2 or lm_1 -EU1 with an erosive or sharp contact (Figs. 6B–6D), and it ranges in thickness from 0.5 to 5 m. It is gray in color and very similar to lm_1 -EU1 (lithofacies mALB, mAL; Table 1A), but it generally shows higher fines content, a slightly more heterolithic nature, and pale brown pumice, yellowish-brown hydrothermally altered medium lapilli, and soil rip-up clasts. At its thickest, the unit contains a few small gas pipes, and the upper parts of the deposits are weakly pinkish oxidized. Poorly sorted grain-size distributions are polymodal to bimodal, mesokurtic to platykurtic, and mostly symmetrical, except at the most proximal (DJ-68) and most distal (DJ-91) locations, where these are positive skewed (Supplemental Materials 1.2 and 1.3). The lithofacies mALB of lm_1 -EU3 is commonly found on the topographic surface along interfluvial areas between the Humadal stream and the Resina River, and (locally) between the Carmelo and Florida streams, directly overlying the paleosol on the Ánimas pumice fallout, or above the older hu_1 or hu_m members. On top of higher Pleistocene terraces at Las Mesas village, the basal portion of lm_1 -EU3 (~20–80 cm thick) shows low-angle cross-stratification (lithofacies xsAL, xsLA; Table 1A), laterally changing to laminated and massive ash (lithofacies IA, mA; Table 1A). Laterally, lm_1 -EU3 changes into a finer-grained massive ash and lapilli bed with abundant accidental lithics (lithofacies mAL; Table 1A; Fig. 6B).

Over distance and on top of the high Pleistocene terraces, exposures comprise a bedded succession of two 2–3-m-thick beds of massive ash and lapilli (lithofacies mAL; Table 1A), separated by a thin (5 cm), weakly cross-stratified ash and lapilli bed (lithofacies wxsLA; Table 1A). Unit lm_1 -EU3 is the most widespread

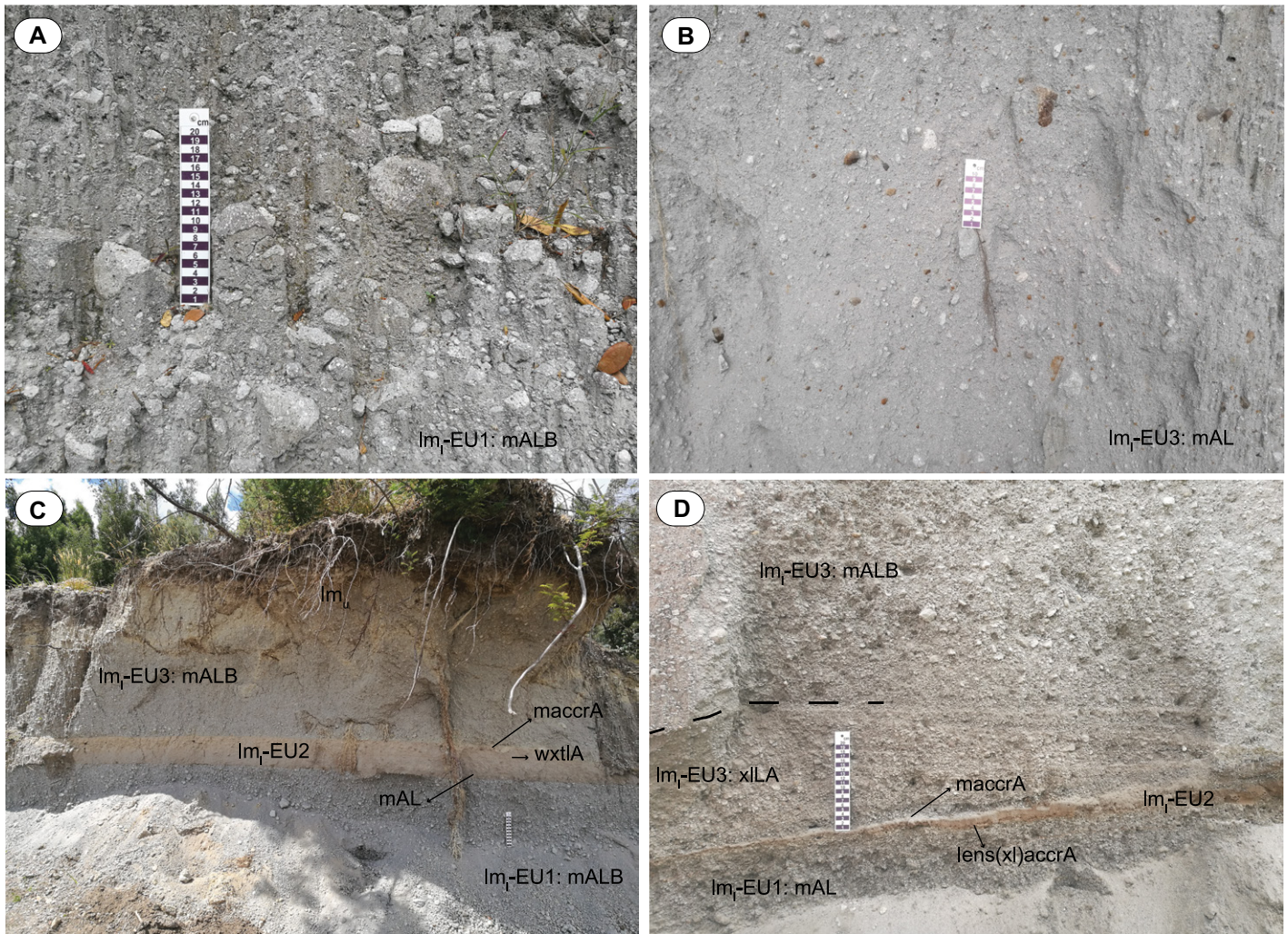


Figure 6. Typical lithofacies associations of pyroclastic density current deposits related to Vulcanian eruptions, reconstructed from the lower member (lm_1) of Las Mesas formation: (A) massive lithofacies at DJ-07; (B) massive lithofacies at DJ-37; and (C–D) exposures of distinct eruption units (EU1–EU3) of lm_1 member, mostly located around the Las Mesas village. Note the distinctively fine-grained nature of lm_1 -EU2. Lithofacies codes are described in Table 1. See Supplemental Material 1.1 (text footnote 1) for referenced locations.

unit of the lm_1 member, exposed down to 10 km from the volcano summit. In general, matrix grain-size distributions of lm_1 -EU1 and lm_1 -EU3 massive lithofacies show $-2.4 < D_{50}(\varphi) < 0.11$ and higher coarse ash contents (23–68 vol%) than fine ash content (0–16 vol%). Radiocarbon dating from charcoal fragments within lm_1 -EU3, reported by Pardo et al. (2019), gave ages of 3052 ± 22 yr B.P. (3351–3207 cal. yr B.P.) and 3018 ± 23 yr B.P. (3265–3148 cal. yr B.P.), largely overlapping with those of the other eruption units.

Eruption unit lm_1 -EU4. The uppermost unit lm_1 -EU4 is local and discontinuous, consisting of clast-supported horizons of dense, gray to brown, vesicular, dacitic, angular medium to fine lapilli (lithofacies mL; Table 1A). At only one location (DJ-25), these deposits mantle unit lm_1 -EU3. Other isolated and discontinuous horizons

of clast-supported angular lapilli are commonly found at the base of the thick soil profile developed on top of the Ánimas fallout marker along the road connecting Las Mesas village to La Cruz town. Although the stratigraphic position and lithology match Las Mesas formation, such middle-distance deposits could not be assigned to a specific eruption unit.

Based on the radiocarbon dates revisited here (Supplemental Material 2), the Las Mesas formation is coeval with the 2860 ± 30 ^{14}C yr B.P. (3072–2877 cal. yr B.P.) La Cabaña formation reported by Pardo et al. (2019) as the only one related to the Young Doña Juana summit vent area to the northwest of Doña Juana volcanic complex (outside our study area; Fig. 3). The pyroclastic deposits of La Cabaña formation correspond to a massive and poorly sorted, monolithologic red tuff-breccia (lithofacies $mALB_{[ij]}$; Table 1A).

Upper Member (lm_u)

This volcanoclastic member is locally exposed along the Humadal stream, overlying or juxtaposed at lower elevations against the lm_1 member. The lm_u member comprises 4–8-m-thick successions of massive to weakly reversely graded beds of very poorly sorted to poorly sorted, heterolithic (gray >> red dacites > accidental lithics) sandy-muddy gravels and gravelly muddy sands (lithofacies $mGSM_{[rg]}$, $mSGM$; Table 1B). Gravels show variable roundness and are locally imbricated within a hardened and porous silty-clayish matrix.

On the terrace where the Las Mesas village is located, the lm_u member is finer grained than the channel-filling lithofacies, and it is represented by a 30–50-cm-thick, pale yellow-brown, lensoid, muddy-gravelly sand bed (lithofacies $mSMG$; Table 1B) capped by a 30–70-cm-thick, dark brown paleosol.

Silencio Formation

This unit encloses the deposits of the late nineteenth century eruption episode, draping the previous units. It extends from the base of the Young Doña Juana lava dome field apron and along the Hueco Seco stream to the southwest, forming a smooth volcaniclastic lobate landform hosting young vegetation (Figs. 2–4 and 7A). Some outcrops also occur along the Carmelo and Florida streams, overlying the Las Mesas formation. Intermediate to distal outcrops occur along the Humadal stream valley close to its outflow into the Resina River, and on top of high Pleistocene terraces close to the Las Mesas village.

The Silencio formation consists of a pyroclastic lower member (si_l) and a volcaniclastic upper member (si_u).

Lower Member (si_l)

This is a pyroclastic succession that is subdivided into four eruption units (si_l EU1–EU4) by means of distinctive lithofacies and locally interbedded reworked deposits (Fig. 3). The composition of juvenile clasts is the most narrow ($64.73 < SiO_2 \text{ wt\%} < 65.84$) of the studied deposits.

Eruption unit si_l -EU1. Proximal outcrops of unit si_l -EU1 are within the vc_2 caldera (DJ-74) and consist of massive, poorly sorted deposits of lapilli and blocks within a lithic-crystalline to

vitric-crystalline, very coarse ash matrix (lithofacies mALB; Table 1A). Unit si_l -EU1 abuts the Las Mesas formation and is best exposed between 4.3 and 8.9 km from the volcano summit, forming discontinuous depositional terraces along the Humadal stream. The thickest outcrops of si_l -EU1 (12–20 m; Figs. 7B and 7C) show coarse-tail graded deposits hosting dense blocks and bread-crust bombs at the base and pumiceous bombs at top (lithofacies mBLA_[g-ct], mALB_[g-ct]; Table 1A). The uppermost portions also contain sparse accidental metamorphic and multicolored hydrothermally altered accessory lithic lapilli. In general, grain-size distributions are polymodal and symmetrical at the base to positive skewed at the top (Supplemental Materials 1.2 and 1.3).

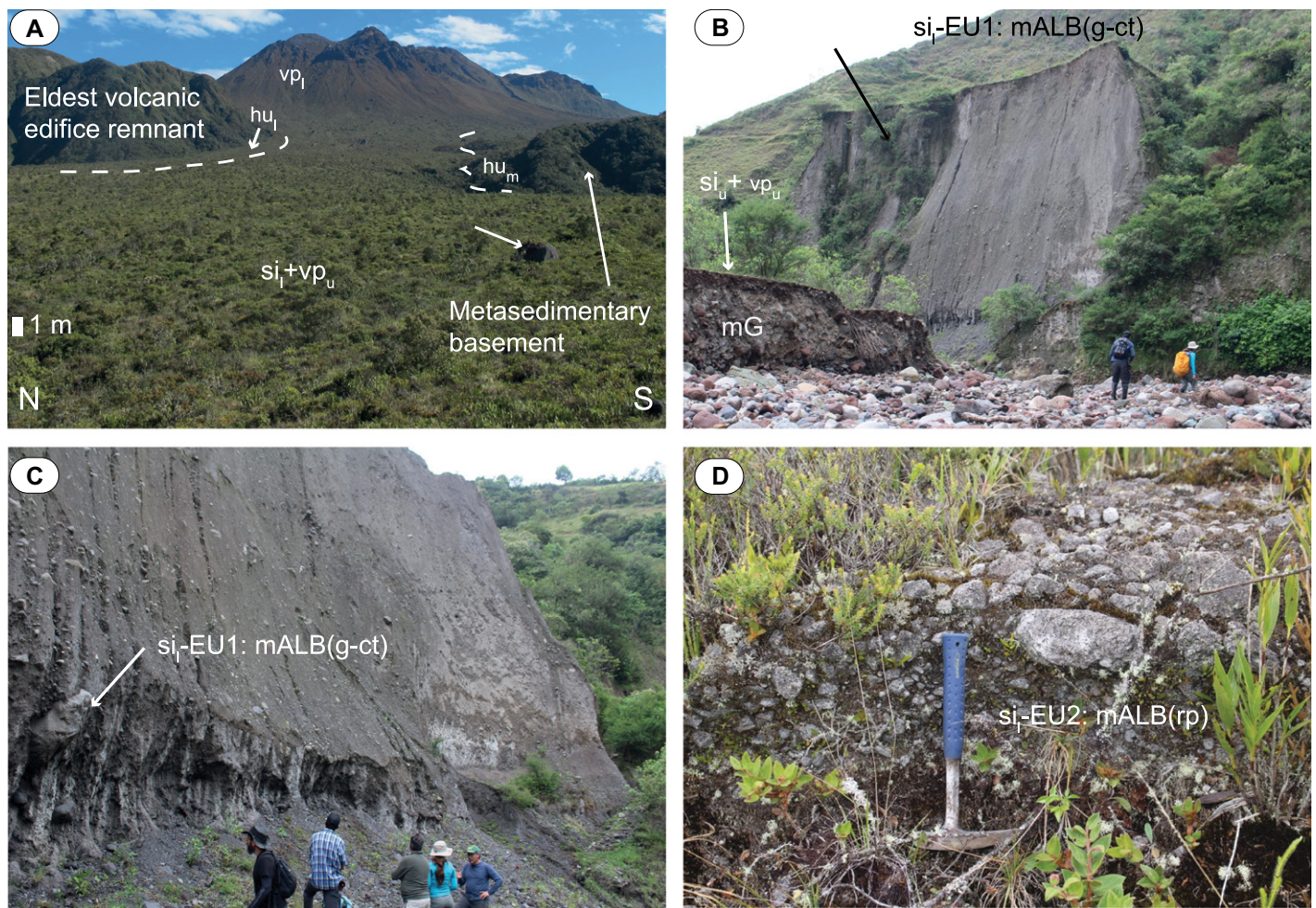


Figure 7. Landscape and exposures of the Silencio formation, distinguished by its high pumice clasts content. (A) Lower member (si_l) deposits smooth the preexisting topography on the southwestern slopes of Young Doña Juana, partially draping remnants of an elder (Pleistocene) edifice, and they are covered by sparse blocks of the upper member (vp_u) of the Valle de Piedras formation (one of them indicated by an arrow). Dashed lines mark the contacts between the Humadal, Silencio, and Valle de Piedras formations. (B–C) Eruption units si_l -EU1 and si_l -EU2 form thick depositional terraces along the Humadal stream, showing coarse-tail reversely graded lithofacies; the white arrow points toward a bread-crust bomb. (D) Proximal exposure of unit si_l -EU2 at the western foothill of the Young Doña Juana lava domes, which shows reverse grading and sometimes is mixed with bread-crust bombs. Lithofacies codes are described in Table 1.

Large charred wood fragments are abundant at the base and provided a new radiocarbon age of 146 ± 21 ^{14}C yr B.P. (1780–1906 CE). Lateral variations were identified at Sofía stream valley, where unit si_i -EU1 thins and overlies fluvial and colluvial deposits found on top of the Las Mesas formation. There, a 1-m-thick bedded unit occurs; its base is a dark gray, massive, lithic-crystalline, very coarse ash showing degassing pipes and transitioning upward into a 12-cm-thick, massive, pale gray, crystalline-lithic medium ash bed (lithofacies mAL; Table 1A) capped by 1–2 cm of massive very fine ash (lithofacies mA; Table 1A). Grain-size distributions are poorly sorted and mesokurtic, changing from positive skewed at the lowermost bed to coarse skewed at the uppermost bed (Supplemental Materials 1.2 and 1.3). Charred branches embedded in unit si_i -EU1 in this sector gave new radiocarbon ages of 125 ± 21 ^{14}C yr B.P. (1802–1937 CE) and 115 ± 21 ^{14}C yr B.P. (1805–1928 CE).

Eruption unit si_i -EU2. Unit si_i -EU2 is a pumice-rich, massive, reddish-gray tuff-breccia that overlaps si_i -EU1 with a sharp erosive contact, best exposed as a distinctive lobe near the base of the Young Doña Juana volcanoclastic apron. Proximal outcrops (DJ-68; 1.7 km from the summit) are reversely graded and contain abundant bread-crust pumiceous bombs forming distinct levees (lithofacies mALB_[rg]; Table 1A; Fig. 7D). Grain-size distributions are polymodal, poorly sorted, and symmetrical and platykurtic at the base to positive skewed and mesokurtic at the top (Supplemental Materials 1.2 and 1.3). In general, the matrix of massive tuff-breccias in units si_i -EU1 and si_i -EU2 shows higher contents of coarse ash (33–87 vol%) versus fine ash (2–25 vol%). Lateral lithofacies variations of si_i -EU2 were identified at overbank environments along the Sofía stream. There, the unit is composed of a 95-cm-thick ash and fine lapilli deposit, where its lowermost and uppermost 10 cm intervals are well-sorted, reddish-gray, weakly cross-stratified and pumice-bearing deposits (lithofacies wxsAL; Table 1A). The intermediate, thicker portion is massive and poorly sorted, with abundant pumice and hydrothermally altered fine lapilli (lithofacies mAL; Table 1A), locally containing gas pipes. In addition, there are bread-crust to cauliflower pumice bombs on the present landscape, down to ~6 km west and southwest from the source, with maximum diameters of 56 cm. A new radiocarbon age was obtained in charred branches within unit si_i -EU2 at 201 ± 21 ^{14}C yr B.P. (1653–1927 CE).

At ~6 km downstream from the summit, units si_i -EU1 and si_i -EU2 are separated by a layer of massive to reversely graded, heterolithic sandy-muddy gravels (lithofacies mG, SM_[rg], mSGM; Table 1B) of the si_u member. Charred

trees within the latter were dated by Pardo et al. (2019) to 127 ± 25 ^{14}C yr B.P. (1800–1941 CE), likely relevant to reworked material of si_i -EU1.

Eruption units si_i -EU3 and si_i -EU4. These are distinctively clast-supported tephros and are only recognized at location DJ-77 (Supplemental Material 1.1), 5.6 km southwest from the volcano summit, capping a 27-cm-thick deposit of tuffaceous (pumice-bearing), muddy-gravelly sands (lithofacies mSMG, mSM; Table 1B) above unit si_i -EU2. Unit si_i -EU3 is an ~9 cm-thick, discontinuous, poorly sorted (symmetrical, leptokurtic), normally graded, and clast-supported (subangular) pumice lapilli and coarse ash gray horizon (lithofacies mL, mA; Table 1A), whereas unit si_i -EU4 is a 2–4-cm-thick, moderately to well-sorted (positive skewed, mesokurtic), pumiceous, very coarse ash bed (lithofacies mA; Table 1A). Units si_i -EU3 and si_i -EU4 are capped with transitional contacts by ~30–40-cm-thick, brown, tuffaceous, muddy-gravelly sands belonging to the si_u member (lithofacies mSMG; Table 1B).

Distal deposits of the si_i member were identified on the high Pleistocene terrace hosting the Las Mesas village, 10 km from the volcano summit. There, the si_i member is locally represented by whitish, discontinuous patches (<6 cm thick) of massive ash or aligned angular pumice fine lapilli within the uppermost soil profile (lithofacies mA; Table 1A), which cannot be attributed to a particular eruption unit.

Upper Member (si_u)

This volcanoclastic member interfingers with the pyroclastic member, and it is also recognized at the junctions of Hueco Seco stream, Humadal stream (Fig. 7B), and Sofía stream with the Resina River (~3–8 m thick). There, massive to weakly reversely graded heterolithic gravels and sandy-muddy gravels of variable roundness form low depositional terraces (lithofacies mG, mGSM_[rg], mSGM; Table 1B) beside the si_i member. In addition, and locally on top of the coarse-tail graded, si_i -EU1 depositional terrace at the outflow of Humadal stream into Resina River, there is a thinly laminated deposit of well-sorted silt and clay, alternating in color from pale gray to pinkish brown (lithofacies altSC; Table 1B).

Valle de Piedras Formation

This unit includes the predominantly lava products of the effusive activity reported during 1897–1936 CE (Table 2). It includes a lower lava member (vp_l) and upper volcanoclastic member (vp_u).

Lower Member (vp_l)

The lower member comprises the endogenous dacitic ($65.06 < \text{SiO}_2 \text{ wt\%} < 65.58$)

lava domes and spines forming the Young Doña Juana volcano summit, together with their surrounding blocky talus aprons (Figs. 2, 3, and 8A). At least five different eruption units (vp_l , EU1–EU5) were recognized by means of cross-cutting relationships and deformation structures. The oldest unit, vp_l -EU1, corresponds to the eastern-northeastern lava dome remnants crosscutting the eastern Phyllo and northeastern Totoral lava domes (Fig. 2). It is composed of fractured porphyritic dacites with irregular foliation and blocky surfaces, forming a semicupola exposed at the eastern side of the lava dome field. Its surrounding monolithologic talus apron drapes the base of the elder Phyllo and Totoral lava domes, as well as the Las Mesas formation within the vc_2 caldera. At a similar stratigraphic position, but not in direct contact, unit vp_l -EU2 is another lava dome remnant and surrounding apron, which is partially exposed in the northwestern portion of the Young Doña Juana lava dome field (Fig. 2). This lava dome has several spines, which are partly plastered by a deposit of hydrothermally altered lithic and angular fine blocks and coarse lapilli (Fig. 8B; lithofacies mL in Table 1A). Both the vp_l -EU1 and vp_l -EU2 lava domes are cut by the highest cusped lava dome of vp_l -EU3, which is almost entirely covered by a talus of lava blocks, and it deforms the earlier and lithic-covered lava spines (Fig. 8C). Most of the vp_l -EU3 talus is exposed to the north-northwest of the Young Doña Juana lava dome field, and meter-sized dacitic blocks fill the valley between the vp_l -EU1 and vp_l -EU3 domes. A younger extrusion is represented by the lava spines of vp_l -EU4 crosscutting the previous units along the rim of the summit lava dome field (Figs. 8C). The corresponding apron is exposed to the west, draping the vp_l -EU1 and vp_l -EU2 talus (Fig. 2), and overlapping the Silencio formation. Finally, an inflated, cracked protrusion (Fig. 8D), named by the locals as the “*papa*” (i.e., Spanish term for “potato”), represents the latest lava dome, vp_l -EU5. This inflated dome deforms the preexisting top of vp_l -EU2.

Upper Member (vp_u)

The upper member is a volcanoclastic deposit comprising sparse, meter-sized angular megablocks (Figs. 7A and 8E), together with monolithologic, massive or reversely graded breccias forming levees (lithofacies mB_[rg]; Table 1A). The vp_u member is interlayered within the talus blocky apron of the vp_l -EU4 dome (Fig. 7A), and it forms a distinctive hummocky topography (grass-covered) extending 4.5 km from the volcano summit. Further down the outflow of this apron into the Resina River, the vp_u member changes into hard, massive,

TABLE 2. INTEGRATION OF THE GEOLOGIC RECORD AND HISTORICAL CHRONICLES FOR THE 1897–1936 CE ERUPTION EPISODE

Historical chronicles	Inferred processes and evidence in the geologic record
<u>1 and 2 November 1897</u> Noise and igneous glow.	Minor Vulcanian explosions accompanied major lava dome growth phases that are hard to distinguish in the geologic record.
<u>6 September 1898</u> Eruption with thunder and incandescence, lasting several days, with lava dome growth accompanied by violent explosions.	
<u>20 April 1899</u> "Fire clouds," "lava and hot ash" flowing down the river valleys, causing "more than 33 casualties" in Las Mesas village. The landscape was "completely perturbed along 3 leagues" (i.e., ~14.5 km from source).	Vulcanian-type to subplinian eruption column, ejecting ballistics (pumice bread-crusteds bombs in Silencio formation), and accompanied by column-collapse pyroclastic density currents (PDCs) running through the main valleys. The two 1899 major events correspond to the PDCs recorded in eruption units sil-EU1 and sil-EU2. Lehmans' report fits with the dominant wind directions in the study area as derived from the nearest information within the national wind atlas (http://atlas.ideam.gov.co/visorAtlasVientos.html)
<u>13 November 1899</u> The "worst" eruption occurred; 50–60 people were "burned by hot blocks and ashes" and Las Mesas village was abandoned. This event started in the morning with strong gas emission, followed suddenly by a "gigantic column that exploded from all sides," producing "igneous clouds," resembling "a castle of fireworks." Locals described "incandescent material falling over the landscape" and "bright ejecta that came out of the column travelled a great distance, some falling to the ground causing fires." It was reported that "a thick rain of ash began to fall and covered the sun, sinking everything in darkness," and "about 5:30 pm, the day began to clear up again." Witnesses described a buoyant eruption column ascending to >20 km, producing an extensive ash plume dispersed to the north, and lasting at least for 5.5 h. Ash was reported by Friedrich Karl Lehmann, who was the German consul in Colombia at the time (Küch, 1892), down to the towns of Guapi and Timbiquí (~170 km to the NW), Buga (~275 km to the N), and Inzá (~150 km to the NNE). A "nueé ardente" flowed down the Resina River valley towards the southwest for 10 km from the source, and a smaller current flowed down to the western flanks (unpublished reference of Hantke and Parodi in 1966, reported by Espinosa, 2012). "The Resina stream was dammed for fifteen days," and, once it failed, a flood "swept the fields and large tracts of land" before damaging an old bridge across the Juanambú River. Las Mesas village was abandoned. "The growing lava-dome was suddenly blasted by following explosions until 1906." Although the precise timing of these events could not be confirmed, there are written descriptions of "distinguishable living lava" and "ash puffs" in 1905 (Pereira-Gamba, 1919).	Also, the geologic record records a volcaniclastic (lahar) deposit interbedded between si _i -EU1 and si _i -EU2. These processes correspond to one of the major lahars recorded in the volcaniclastic deposits of the upper member of the Silencio formation, likely the one stratigraphically above si _i -EU2. Early dome growth events/phases recorded in the Valle de Piedras formation. Eruption units sil-EU3 and sil-EU4 show that two minor tephra fallouts occurred to the west, reaching at least 6 km from the vent.
<u>1936</u> Regional tectonic earthquakes were documented (MW 5.6 on January 9 and a swarm between July 14 and 18, with a MW 6.3 shake on July 17), with epicenters located 90 km SW of the volcano. Nearly a month later, at 5 am of 14 August 1936, an "avalanche" triggered from the summit killed >23 people and caused losses of crops and livestock (El Derecho, Pasto, 8/15/1936 and national newspapers). "The landslides have an extension of no less than a league and a large part of them fell on the lagoons, displacing the water they had and even the mud through the Resina stream, which became in a few moments a mighty river, then passing that flow to the Juanambú River." "Both in the place where the lagoons used to be, as in the entire route of the Resina [River], there are immense extensions of mud that seem to be volcanic with a strong smell of sulphur. The area of the lagoons is also covered with stones of incredible dimensions, which seem to have detached from the volcano." [...] "likewise, hikers verified that landslides continued for several days" (El Derecho, Pasto, 8/22/1936).	Partial collapse of the summit lava dome spines, rock avalanche, and subsequent debris flow interpreted here from the Valle de Piedras formation.

Note: Chronicles were mainly taken from Küch (1892), Pereira-Gamba (1919), Espinosa (2012), local unpublished essays (Gómez-Bolaños, 2012), national newspapers (i.e., El Espectador, 1887; El Herald, 1899; El Derecho, 1936; El Tiempo, 1936, and interviews with elders (Pulgarín et al., 2015; Arnulfo Bravo, 2015; María Mercedes Muñoz, 2015; Delfina Muñoz, 2015, 2017, personal communications).

heterolithic gravels or local superpositions of reversely graded, sandy-muddy gravels (lithofacies mG, mGSM_[reg]). These deposits form 6-m-high depositional terraces at the intersection of the Sofía stream and Resina River, which are difficult to distinguish from the earlier si_i member (Fig. 8E). Overall, no pumice clasts were found within the Valle de Piedras formation.

DISCUSSION

Eruption Styles and Chronology

The new stratigraphic reconstruction allowed us to identify different eruption epi-

sodes related to the Young Doña Juana central vent area in the late Holocene (Figs. 9 and 10A), with at least three main explosive eruption episodes ca. 5 cal. k.y. B.P. (Humadal), ca. 3 cal. k.y. B.P. (Las Mesas), and 1897–1936 CE (Silencio–Valle de Piedras). These occurred simultaneously or alternating with the activity described by Pardo et al. (2019) for the adjacent vent areas, (1) Phyllo and (2) Totoral (Figs. 2 and 3).

The late Holocene Young Doña Juana produced alternating effusive and explosive eruptions (Fig. 9), typical of many dome-forming volcanoes (e.g., Samaniego et al., 1998; Platz et al., 2007, 2012; Lerner et al., 2019; Massaro et al., 2019). Modern dacitic analogues show-

ing eruption transitions without development of Plinian phases include Cayambe (Samaniego et al., 1998), Imbabura (Andrade et al., 2019), Soufrière Hills (Druitt et al., 2002; Formenti et al., 2003; Burgisser et al., 2010; Gottsmann et al., 2011), Mount Unzen (Nakada and Fujii, 1993), and Mount Merapi (Cronin et al., 2013). These contrast with similar dacitic lava dome systems that also produce Plinian eruptions, like Mount Peleé (Fisher and Heiken, 1982) or Volcán de Colima (Sulpizio et al., 2010; Capra et al., 2016; Pensa et al., 2018).

5 cal. k.y. B.P. Humadal Eruption Episode

This episode is represented by successive block-and-ash flows produced by lava

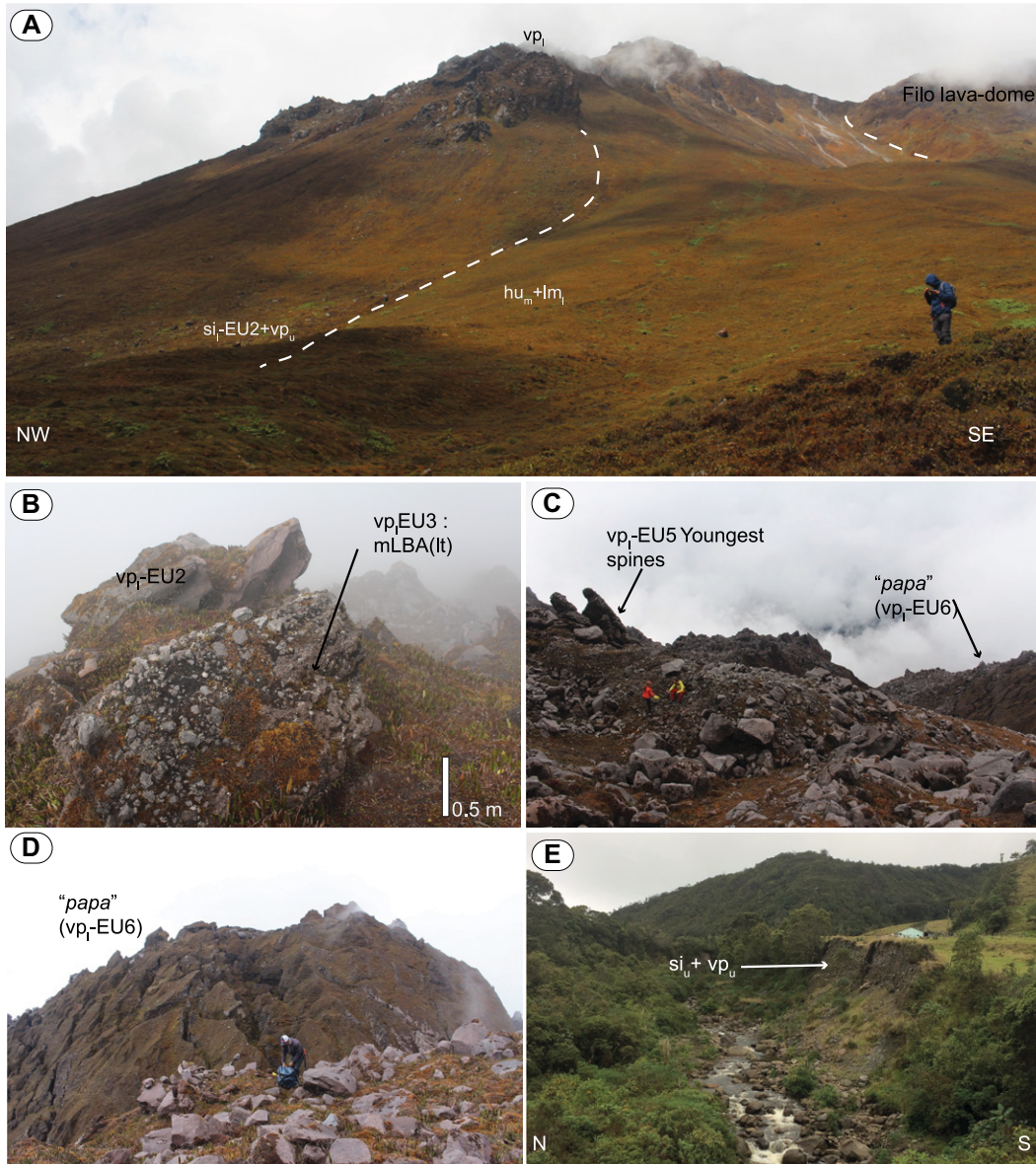


Figure 8. Landscape and exposures of the Valle de Piedras formation. (A) Lower member (vp_l) forms the summit lava dome complex at the central vent zone. (B–C) Lobate and spiny lava domes surrounded by blocky aprons of the vp_l -EU1 and vp_l -2 eruption units. (D) Latest lava dome of unit vp_l -EU5 inflating below and deforming older lava domes. (E) Depositional terraces of the latest lahar deposits at the upper Resina River, including the ones subsequent to the 1899 CE eruption (si_u member, Silencio formation) and the 1936 CE rock avalanche (vp_u member, Valle de Piedras formation).

dome collapses, a pyroclastic density current generated by lava dome explosion (Boudon et al., 2015) and pyroclastic fountain collapse, and subsequent lahars. The valley-confined, massive to weakly reversely graded, poorly sorted, and monolithologic lithofacies associations of the hu_l member (lithofacies mBLA, $mB_{[jw]}LA_{[rl]}$, $mBLA_{[rl]}$, $mALB_{[rl]}$; Table 1A) support deposition from block-and-ash flows (Supplemental Material 1; Figs. 10B and 10C). The matrix grain-size distributions indicate that the bulk of the material was transported within the high-density ground-hugging basal part of the current (e.g., Schwarzkopf et al., 2005). The superposition of weakly reversely graded beds indicates that grain-grain interaction in a granular flow depositional regime favored kinetic sieving (Savage and Lun, 1988) and kinematic

squeezing (Le Roux, 2003), which segregated the largest blocks to the top of the flows. Their homogeneous reddish color indicates syneruptive oxidation of the collapsed lava domes due to temperature, which means that they were likely extruded at a higher temperature compared to the successive ones. The vertical repetitive occurrences of reversely graded lithofacies and horizons of flat-lying blocks parallel to the base indicate either the stepwise aggradation of different pulses developed within the same block-and-ash flow or the recurrence of multiple, discrete dome collapses in a short time generating successive block-and-ash flows (e.g., Sulpizio et al., 2007, 2014; Sulpizio and Dellino, 2008; Lucchi et al., 2022). Deposition from successive pulses is best recorded in the Carmelo catchment area, where the low-angle

cross-laminated deposits (lithofacies sLA) suggest traction and deposition from a turbulent regime in the dilute region at the top of each high-concentration block-and-ash flow pulse (Macorps et al., 2018).

The sedimentologic data from the hu_m member (lithofacies $mBLA_{[rl]}$ and $mALB$) suggest rapid deposition from the underflow of concentrated pyroclastic density currents dominated by granular flow depositional regimes (Figs. 10B–10C). No fall deposits were recognized, suggesting the pyroclastic density currents were generated from the collapse of low pyroclastic fountains associated with ballistic ejection of bread-crusts bombs. The presence of bombs, pumice, and accidental lithic clasts indicates explosive disruption of a lava plug/dome and the fragmentation of metamorphic

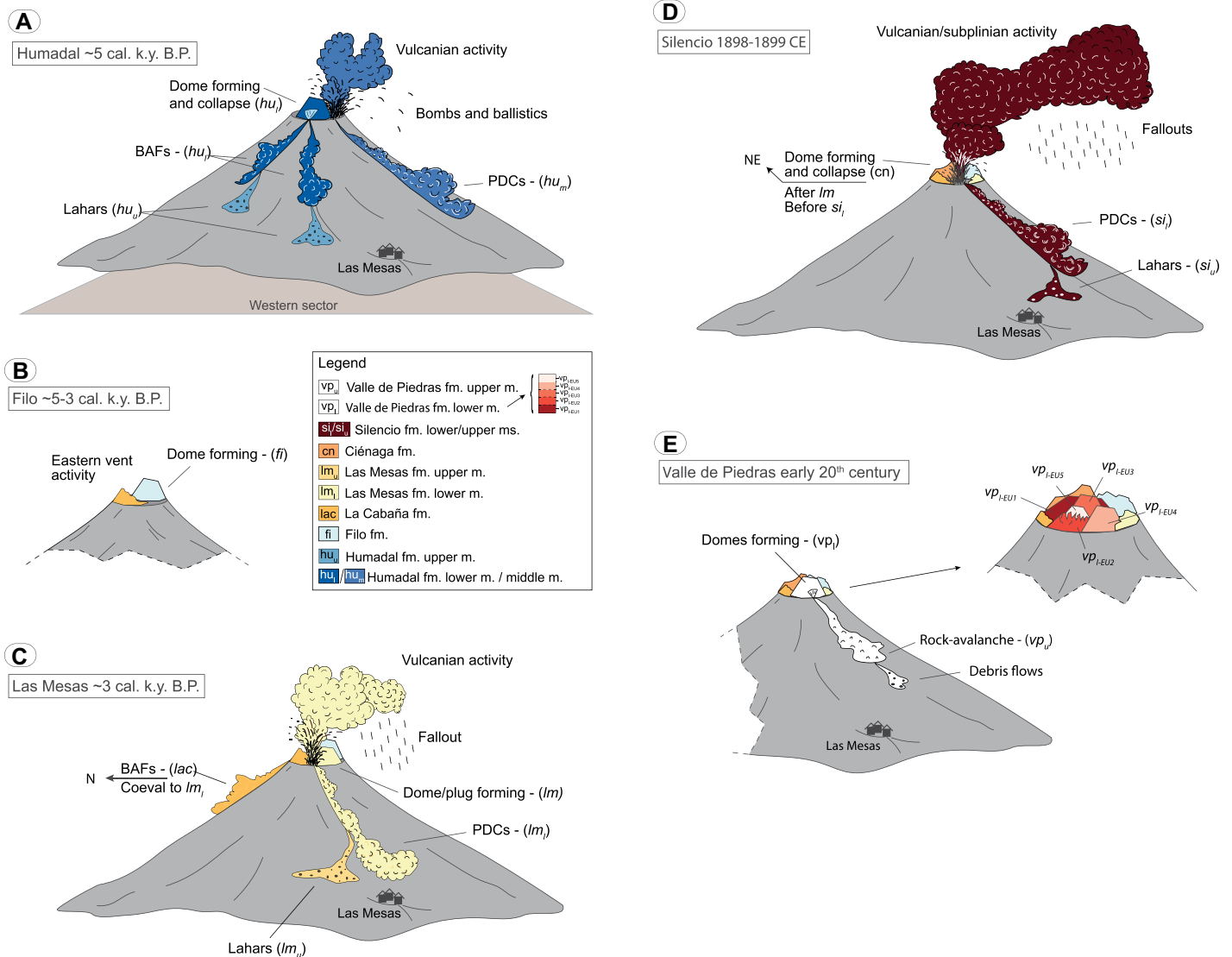


Figure 9. Simplified sketch showing the evolution of the youngest Doña Juana lava dome complex, including Phyllo, Totoral, and Young Doña Juana vent zones. The explosive activity has been concentrated at the latter eruptive source. In chronological order: (A) lava dome collapse block-and-ash flows (BAFs) inferred from the Humadal formation, as well as Caicuanes and Ciénaga formations reported by Pardo et al. (2019); (B) effusive phases at the easternmost vent area (Phyllo formation); (C) lava dome collapse block-and-ash flows and Vulcanian pyroclastic density current (PDC) products inferred from Las Mesas formation; (D) violent Vulcanian to subplinian(?) pyroclastic density current, as inferred from Silencio formation; and (E) dominantly effusive activity products inferred from the Valle de Piedras formation. All eruption episodes, except those related to Phyllo vent, included syneruptive or posteruptive lahars.

country rock (e.g., Benage et al., 2014; Macías et al., 2020). The estimated minimum total bulk volume for the combined pyroclastic hu_1 and hu_m members of the Humadal formation is $9.7 \times 10^6 \text{ m}^3$.

The massive to weakly reversely graded, heterolithic, coarse-grained deposits of the hu_u member (lithofacies $mGSM_{[rg]}$; Table 1B) are interpreted as debris-flow deposits reworking the hu_1 pyroclastic member along the main river valleys. Mud-rich lithofacies $mSMG$

and mSM are interpreted as mudflow deposits (Fig. 9A).

Ca. 3 ka Las Mesas Eruption Episode

This episode was characterized by lava dome collapses, plug removal upon Vulcanian explosions, low columns that partially or totally collapsed producing pyroclastic density currents, and lahars. The componentry of both the lm_1 -EU1 and lm_1 -EU3 eruption units indicates explosive disruption of a lava plug or

a fresh lava dome (Fig. 9B), expelling mostly dense to poorly vesicular juvenile materials. The presence of metamorphic lithics indicates that the fragmentation depth reached the country rock or that the violence of the eruption favored conduit erosion. Matrix-poor massive lithofacies associations $mALB$, mAL , and $lensL$ (Table 1A) of lm_1 -EU1 and lm_1 -EU3 suggest rapid deposition from the underflow of highly concentrated pyroclastic density currents, with a granular flow dominated

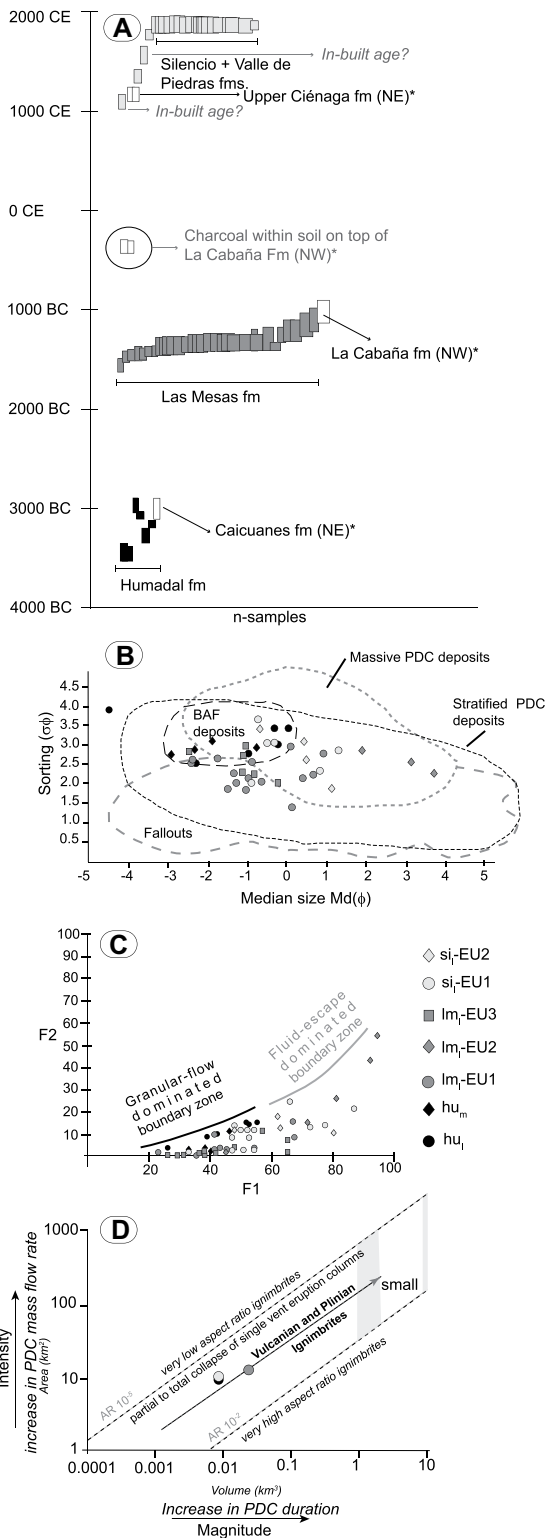


Figure 10. Geochronologic and granulometric summary. (A) Calibrated radiocarbon ages ($n = 67$) obtained with IntCal20 curve (OxCal 4.4; Reimer et al., 2020) from charcoal in each pyroclastic member. The ~2 k.y. gaps correspond to time periods of volcanic quiescence or lava dome growth phases (not datable by C¹⁴). See the corresponding data in Supplemental Material 2 (text footnote 1). *Units reported by Pardo et al. (2019). (B) Walker et al. (1971) diagram showing the Md_{ϕ} vs. σ_{ϕ} parameters obtained from the grain-size analysis. Most data fit within the expected field for massive block-and-ash flows (BAFs) and column-collapse pyroclastic density current (PDC) deposits, particularly for the lm_1 -EU1 and lm_1 -EU2 units of the Las Mesas formation. (C) F1 (particles smaller than 0ϕ) vs. F2 (particles smaller than 4ϕ) plot. Deposits rich in fines mostly correspond to lm_1 -EU1 and lm_1 -EU2 of Las Mesas formation and contain F2 > 20 wt%. Lithofacies codes are described in Table 1. (D) Classification diagram of Giordano and Cas (2021).

flow-boundary zone (Figs. 10B–10C). Matrix-rich lithofacies were deposited in a fluid-escape depositional regime zone (Figs. 10B–

10C) at high clast concentration, during which gas retention within the granular mixture was a function of the porosity of the moving mix-

ture. The occurrence of gas pipes in places supports the presence of high quantities of gas in the eruptive mixture at the time of deposition. The distinctive reddish-brown lm_1 -EU2 deposits (lithofacies mAL; Table 1A) indicate rapid deposition and fines entrapment, where the common occurrence of charred woods and local tanned pink colors likely indicate high temperatures of emplacement. The rip-up soil intraclasts reflect the erosional capability of these currents, particularly for the uppermost lm_1 -EU3. The channelized flows of lm_1 -EU1 and lm_1 -EU3 were able to overtop high elevations, with slightly increasing fines content and improved sorting toward the front, where two depositional flow pulses were recorded. There, and in overbank environments, the lowermost cross-stratified portions (lithofacies x1A, xsAL, xsLA, wxsLA; Table 1A) suggest grain-by-grain deposition from the basal turbulent zone in a flow boundary dominated by traction at the pyroclastic density current front. Upward transitions in lm_1 -EU2 at overbank environments to weakly stratified or laminated deposits (lithofacies wsLA, wLA, wx1A; Table 1A), and embedded clast-supported lapilli lenses (lensL) suggest enhanced turbulence upon current dilution. The massive and thinly laminated ash (lithofacies 1A, mA, maccrA; Table 1A) found at top of each unit reflects current waning and subsequent settling from elutriated (decoupled?) ash clouds. In addition, the poorly preserved clast-supported (angular) lapilli beds (lithofacies mL; Table 1A) represent remnants of fall deposits, thus supporting the hypothesis of low-column-collapse-derived pyroclastic density currents. The total estimated (minimum) volume for the pyroclastic density current deposits of the lm_1 member is $24.0 \times 10^6 \text{ m}^3$.

The massive and monolithic tuff-breccias (lithofacies mALB) of the coeval La Cabaña formation reported by Pardo et al. (2019) outside the study area, but which also originated at the central Young Doña Juana vent, reflect the accumulation of block-and-ash flow pulses to the north. Whether these flows occurred as opening phases or were synchronous with Las Mesas formation deposition remains unclear due to the absence of stratigraphic relations in the field between the two units.

The coarse-grained volcaniclastic deposits of the lm_4 member (lithofacies mGSM_[rg]; Table 1B) are interpreted as debris-flow deposits, while matrix-rich mSMG lithofacies correspond to sand-rich mudflow deposits, both reworking the pyroclastic deposits of the lm_1 member (Fig. 9C). The capping paleosol, together with correlative discontinuous 2–3-m-thick colluvial and fluvial deposits, and a proximal angular unconformity

(Fig. 8A), marks a significant period of quiescence between the Las Mesas formation and the overlying Silencio formation.

1897–1936 CE Silencio–Valle de Piedras Episode

This episode records lava dome/plug disruptions developing violent, partially to totally collapsing Vulcanian to subplinian columns that generated pyroclastic density currents and lahars; this predominantly explosive activity transitioned into successive lava dome and spine extrusions that gravitationally collapsed, generating a rock avalanche and subsequent lahar. Pumice-bearing, massive tuff-breccias (lithofacies mALB) described for the si_1 -EU1 and si_1 -EU2 units of the Silencio formation indicate deposition from the underflow of high-concentration pyroclastic density currents (Figs. 10B–10C). Proximal reversely graded levees (lithofacies mALB_[rp]) and coarse-tail graded lithofacies (mBLA_[g-ct], mALB_[g-ct]) suggest strong density segregation within the currents. Lateral variations at overbank environments were found at the edge of the southwesternmost apron reaching Sofía stream (DJ-10; Supplemental Material 1.1). There, the occurrence of lithofacies mAL (Table 1A) in unit si_1 -EU1 indicates rapid deposition from valley-confined pyroclastic density currents dominated by a fluid escape flow-boundary zone, followed by current waning. The occurrence of lithofacies wxsAL at the base and at the top of unit si_1 -EU2 indicates deposition from a traction-dominated flow-boundary zone at the front and at the end of the main concentrated pyroclastic density current body. The total minimum volume of the pyroclastic density current deposits for the whole si_1 member, calculated using the available data, is $8.7 \times 10^6 \text{ m}^3$.

The occurrence of clast-supported lithofacies mL and mA in units si_1 -EU3 and si_1 -EU4 records at least two fallout depositional phases from an associated eruptive column (Fig. 9D). It is clear that the Silencio activity indicates higher explosivity involving a deeper level of the conduit than the Humadal and Las Mesas eruption episodes. However, we do not have enough elements to confirm a progressive transition into open-conduit conditions.

The heterolithic lithofacies mSMG and mSM of the si_1 member indicate lahars reworking previous pyroclastic deposits. Local occurrence of lithofacies altSC (Table 1B) suggests formation of ephemeral ponds in distal overbank areas.

The vp_1 member of Valle de Piedras formation suggests at least five subsequent phases of growth of the summit lava domes and spines (vp_1 EU1–EU5; Fig. 9E). The total minimum volume of the lava domes currently exposed at the

Young Doña Juana summit area is estimated as $6.8 \times 10^8 \text{ m}^3$, subdivided as follows: $\sim 4.3 \times 10^8 \text{ m}^3$ for vp_1 -EU1, $\sim 5.7 \times 10^4 \text{ m}^3$ for vp_1 -EU2, $\sim 1.3 \times 10^5 \text{ m}^3$ for vp_1 -EU3, $\sim 2.4 \times 10^8 \text{ m}^3$ for vp_1 -EU4, and $\sim 9.5 \times 10^6 \text{ m}^3$ for the youngest (endogenous) vp_1 -EU5.

The monolithic hummocky breccias and sparse blocks described for the vp_u member suggest the accumulation of a rock avalanche where kinetic sieving was important in forming reversely graded deposits. This event likely resulted from the gravitational collapse of one or more lava domes/spines among the most recent ones in the summit lava dome field (Fig. 9E). Similar partial collapses of lava domes have been reported at Soufrière Hills by Watts (2002) and Stinton et al. (2014). The abrupt change to heterolithic gravels at the break in slope, 1.4 km from the lava spines representing the likely source area, reflects the transformation of the rock avalanche into a debris flow.

In the case of the Silencio–Valle de Piedras eruption episode, we can integrate our geologic data with the available historical chronicles (Table 2). Brief written communications within national and regional journal repositories describe ballistic ejection during minor Vulcanian explosions and lava dome growth in 1897–1898, followed by two major paroxysms with ash dispersal beyond $\sim 150 \text{ km}$ and a subsequent lahar in 1899 (Table 2). Historical chronicles also indicate that some seismic events occurred over the following decades, but they could not be confirmed by other sources as accompanying volcanic eruptions (Espinosa, 2012) because their dates coincide with major regional tectonic activity noted by the Colombian Geological Survey (<http://sish.sgc.gov.co/visor/>). These events include the MW 8.8 earthquake in 1906 (Pacific coast epicenter: lat 0.99°N , long 79.35°W), the MW 6.2 earthquake in 1923 (southern Nariño epicenter: lat 0.87°N , long 77.78°W , with ash emission reported from Doña Juana volcanic complex 3 h later), and the ML 6.0 earthquake in 1926 (southern Nariño epicenter: lat 0.87°N , long 77.78°W). The final collapse event at Doña Juana volcanic complex was documented in 1936, but we do not know if it occurred during or after the growth of the domes/spines, or if there was an active hydrothermal system. For sure, the studied deposits do not show any evidence for associated explosive activity.

Flow Mobility

The mobility ratio ($\Delta H/L$), based on the height difference (ΔH) and horizontal distance (L) between the source area and the distal limit of the deposit, captures the ability of gravity-driven mass flows to move downslope (e.g.,

Iverson, 1997). The ratio $\Delta H/L$ defines the coefficient of friction for the mass flow (Hayashi and Self, 1992) and reflects the Mohr-Coulomb angle of internal granular friction (Freundt, 1999). The mobility ratio of block-and-ash flows from Young Doña Juana has values of 0.21–0.22 (Supplemental Material 3), similar to parameters calculated for those derived by lava dome collapse in the Soufrière Hills volcano on Montserrat (Calder et al., 1999). For pyroclastic density currents related to column collapse, ΔH depends on whether the source area is assumed to correspond to the volcano summit or to the height where column collapse occurred (Hayashi and Self, 1992). For Young Doña Juana, a column collapse height of 500 m above the volcano summit produces $\Delta H/L$ values from 0.18 (along Humadal stream) to 0.24 (along Carmelo stream) for pyroclastic density currents dominated by dense juvenile material (Las Mesas formation), and between 0.20 (along Humadal stream) and 0.24 (along Hueco Seco stream) for pumice-bearing currents (Silencio formation). Moreover, along Humadal stream, where all studied units occur and can be compared to one another, $\Delta H/L$ is lower for fountain/column-collapse pyroclastic density currents, consistent with slightly longer runout distances ($\Delta H/L = 0.18$ – 0.20) and slightly lower internal granular friction than for block-and-ash flows ($\Delta H/L = 0.21$).

CONCLUSIONS

The Young Doña Juana central vent within the Doña Juana volcanic complex is an excellent example of a dome-dominated, tropical arc volcano. By merging the late Holocene geologic record, radiocarbon ages, and eyewitness chronicles from the late nineteenth and early twentieth centuries, we interpreted the recent past eruption behavior to include: (1) summit lava dome growth associated with occasional (minor) explosions; (2) gravitational lava dome collapses, generating rock avalanches or larger block-and-ash flows reaching $\geq 7 \text{ km}$ from the vent; and (3) deep dome collapses and plug disruptions leading to Vulcanian to subplinian eruptions forming pyroclastic density currents from pyroclastic fountains/column collapses reaching $\geq 10 \text{ km}$ from the vent, with rare pyroclastic fallout reaching $\geq 150 \text{ km}$ (see Table 2). Historical chronicles (Table 2) suggest that cyclic transitions from lava dome growth phases to explosive phases likely occur over 1–2 yr.

Most of the studied pyroclastic density currents veered toward the west and were channeled through a low saddle on the western rim of the vc_2 caldera (Figs. 2 and 7A) and then cascaded into the Humadal stream valley and reached the

inhabited depositional terrace of the Las Mesas village (Figs. 2–4). In addition to this main flow trajectory, most pyroclastic density currents overflowed through other saddles of the vc_2 caldera rim toward the west into the upper valleys of the Florida and Carmelo streams (Fig. 2). Deposition of the studied pyroclastic density currents mostly occurred under granular flow or fluid escape depositional regimes at high clast concentrations (Figs. 10B–10C), had volumes similar to those calculated for Vulcanian eruptions in other volcanoes elsewhere (e.g., Cole et al., 2014; Capra et al., 2016; Albino et al., 2020), and are classified as Vulcanian ignimbrites following Giordano and Cas (2021) (see Supplemental Material 3; Fig. 10D). The absence of traction-dominated pyroclastic density current deposits in the upper slopes of Young Doña Juana suggests limited generation of diluted and turbulent pyroclastic density currents from overpressurized jets at the source. Traction structures occur only sporadically and mostly in overbank regions, related to more diluted conditions and accompanying turbulent ash clouds possibly induced by the interaction with irregular topography. All of these processes were associated with inter- and post-eruptive lahars.

ACKNOWLEDGMENTS

This study was funded by a University of Los Andes FAPA inner grant allocated to N. Pardo, and by the Visiting Researcher fellowship allocated to N. Pardo at Università degli Studi di Bari Aldo Moro (DR no. 3208 of 2018). S. Cronin was supported by the Transitioning Taranaki to Volcanic Future project of the New Zealand Ministry for Business, Innovation and Employment (UOAX1913). The research was included within agreement no. 35–2018 between the Universidad de Los Andes and the Geological Survey of Colombia. We deeply thank Ricardo Vilota, Manuel Chávez, Las Mesas village inhabitants, and the staff of Doña Juana–Cascabel National Natural Park for their lessons and support during fieldwork. The Historical Ecology and Social Memory Research collective (EHMS of the Universidad de Los Andes) and C. Laverde (Geological Survey of Colombia) helped to interpret the historical documentation. Markus Egli directed the work to obtain the radiocarbon ages at the Radiocarbon Laboratory of the University of Zürich (Switzerland). The technical staff of the Geosciences and Mechanical Engineering laboratories of the Universidad de Los Andes, M.A. Arias, E.S. Villamil, L. Acosta, and D.F. Martínez helped with granulometry analyses. Diego Palechor (Geological Survey of Colombia) helped with the setup of the geographic information system geodatabase. Shari van Treeck (Institute of Geosciences and Meteorology, Universität Bonn, Germany) carried out part of the volume calculations. We greatly thank P. Samaniego, an anonymous reviewer, and the associate editor for their constructive suggestions, which helped to optimize the latest version of this manuscript. Part of the publication costs were covered with the funds of the call “PÚBLICA, EXPÓN O FORTALECE TU PRODUCTO DE TRANSFERENCIA” approved by the Vicerrec-

toría de Investigación y Creación of the Universidad de Los Andes, Bogotá, D.C., Colombia.

REFERENCES CITED

- Albino, F., Biggs, J., Escobar-Wolf, R., Naismith, A., Watson, M., Phillips, J.C., and Chigna Marroquin, G.A., 2020, Using TanDEM-X to measure pyroclastic flow source location, thickness and volume: Application to the 3rd June 2018 eruption of Fuego volcano, Guatemala: *Journal of Volcanology and Geothermal Research*, v. 406, <https://doi.org/10.1016/j.jvolgeores.2020.107063>.
- Andrade, S.D., van Wyk de Vries, B., and Robin, C., 2019, Imbabura volcano (Ecuador): The influence of dipping substrata on the structural development of composite volcanoes during strike-slip faulting: *Journal of Volcanology and Geothermal Research*, v. 385, p. 68–80, <https://doi.org/10.1016/j.jvolgeores.2018.11.017>.
- Benage, M.C., Dufek, J., Degruyter, W., Geist, D., Harpp, K., and Rader, E., 2014, Tying textures of breadcrust bombs to their transport regime and cooling history: *Journal of Volcanology and Geothermal Research*, v. 274, p. 92–107, <https://doi.org/10.1016/j.jvolgeores.2014.02.005>.
- Blott, S., and Pye, K., 2001, Gradistat: A grain size distribution and statistics package for the analysis of unconsolidated sediments: *Earth Surface Processes and Landforms*, v. 26, p. 1237–1248, <https://doi.org/10.1002/esp.261>.
- Boudon, G., Balcone-Boissard, H., Villemant, B., and Morgan, D.J., 2015, What factors control superficial lava dome explosivity?: *Scientific Reports*, v. 5, <https://doi.org/10.1038/srep14551>.
- Bronk Ramsey, C., 2009, Bayesian analysis of radiocarbon dates: *Radiocarbon*, v. 51, no. 1, p. 337–360, <https://doi.org/10.1017/S0033822200033865>.
- Burgisser, A., Poussineau, S., Arbaret, L., Druitt, T.H., Hiachetti, T., and Bourdier, J.L., 2010, Pre-explosive conduit conditions of the 1997 Vulcanian explosions at Soufrière Hills Volcano, Montserrat: I. Pressure and vesicularity distributions: *Journal of Volcanology and Geothermal Research*, v. 194, p. 27–41, <https://doi.org/10.1016/j.jvolgeores.2010.04.008>.
- Calder, E.S., Cole, P.D., Dade, W.B., Druitt, T.H., Hoblitt, R.P., Huppert, H.E., Ritchie, L., Sparks, R.S.J., and Young, S.R., 1999, Mobility of pyroclastic flows and surges at the Soufrière Hills volcano, Montserrat: *Geophysical Research Letters*, v. 26, no. 5, p. 537–540, <https://doi.org/10.1029/1999GL900051>.
- Capra, L., Macías, J.L., Cortés, A., Dávila, N., Saucedo, R., Osorio-Ocampo, S., Arce, J.L., Gavilanes-Ruiz, J.C., Corona-Chávez, P., García-Sánchez, L., Sosa-Ceballos, G., and Vázquez, R., 2016, Preliminary report on the July 10–11, 2015, eruption at Volcán de Colima: Pyroclastic density currents with exceptional runout and volume: *Journal of Volcanology and Geothermal Research*, v. 310, p. 39–49, <https://doi.org/10.1016/j.jvolgeores.2015.11.022>.
- Cediel, F., Shaw, R.P., and Cáceres, C., 2003, Tectonic assembly of the Northern Andean block, in Bartolini, C., Buffler, R.T., and Blickwede, J.F., eds., *The Circum-Gulf of Mexico and the Caribbean: Hydrocarbon Habitats, Basin Formation, and Plate Tectonics: American Association of Petroleum Geologists Memoir 79*, p. 815–848, <https://doi.org/10.1306/M79877C37>.
- Cole, P.D., Smith, P.J., Stinton, A.J., Odbert, H.M., Bernstein, M.L., Komorowski, J.C., and Stewart, R., 2014, Vulcanian explosions at Soufrière Hills volcano, Montserrat, between 2008 and 2010, in Wadge, G., Robertson, R.E.A., and Voight, B., eds., *The Eruption of Soufrière Hills Volcano, Montserrat from 2000 to 2010: Geological Society, London, Memoir 39*, p. 93–111, <https://doi.org/10.1144/M39.5>.
- Cortés, G.P., 2011, Observatorios vulcanológicos en Colombia: 25 años de vigilancia ininterrompida, in IN-GEOMINAS al Día: Bogotá, D.C., Colombia, Instituto Colombiano de Geología y Minería, Internal Report, p. 12–25.
- Cortés, M., and Angelier, J., 2005, Current state of stress in the northern Andes as indicated by focal mechanisms of earthquakes: *Tectonophysics*, v. 403, p. 29–58, <https://doi.org/10.1016/j.tecto.2005.03.020>.
- Cronin, S.J., Lube, G., Dayudi, D.S., Sumarti, S., Subrandiyo, S., and Suroño, 2013, Insights into the October–November 2010 Gunung Merapi eruption (Central Java, Indonesia) from the stratigraphy, volume and characteristics of its pyroclastic deposits: *Journal of Volcanology and Geothermal Research*, v. 261, p. 244–259, <https://doi.org/10.1016/j.jvolgeores.2013.01.005>.
- Driedger, C., Calvache, M., Cortés, G.P., Ewert, J., Montoya, J., Lockhart, A., Allen, R., Banks, D., Beason, S., Trujillo-Bocanegra, H., Frances, B., Bustad, K., Gallego, J.A., Gibson, Z., Giraldo, F.R., Gutierrez, C., Quinter, J.L., Rodríguez, E., Schelling, J., and Scott, M., 2020, Leveraging lessons learned to prevent future disasters—Insights from the 2013 Colombia-US binational exchange: *Journal of Applied Volcanology*, v. 9, p. 3, <https://doi.org/10.1186/s13617-019-0090-8>.
- Druitt, T.H., Young, S.R., Baptie, B., Bonadonna, C., Calder, E.S., Clarke, A.B., Cole, P.D., Harford, C.L., Herd, R.A., Luckett, R., Ryan, G., and Voight, B., 2002, Episodes of cyclic Vulcanian explosive activity with fountain collapse at Soufrière Hills volcano, Montserrat, in Druitt, T.H., and Kokelaar, B.P., eds., *The Eruption of Soufrière Hills Volcano, Montserrat, from 1995 to 1999: Geological Society, London, Memoir 21*, p. 281–306, <https://doi.org/10.1144/GSL.MEM.2002.021.01.13>.
- El Espectador, 1887, Nariño quedó incomunicado con la erupción del volcán, Corresponsal de Pasto [National newspaper repository at the library Luis Angel Arango, Bogotá]: *El Espectador*, 22 March 1887.
- El Derecho, 1936a, Fuertes temblores se sintieron el día domingo en varias poblaciones del departamento, Corresponsal [Regional newspaper repository of Centro Cultural Leopoldo López Álvarez del Banco de la República en Pasto, Nariño, Colombia]: *El Derecho*, 8 January 1936.
- El Derecho, 1936b, A última hora “Una erupción del volcán Doña Juana destruyó el puente “Solarte Obando”, Corresponsal [Regional newspaper repository of Centro Cultural Leopoldo López Álvarez del Banco de la República en Pasto, Nariño, Colombia]: *El Derecho*, 15 August 1936.
- El Derecho, 1936c, Jurado, J.F., La verdad sobre la erupción del volcán “Doña Juana” [Regional newspaper repository of Centro Cultural Leopoldo López Álvarez del Banco de la República en Pasto, Nariño, Colombia]: *El Derecho*, 19 August 1936.
- El Derecho, 1936d, Al margen de la vida, La tragedia del Juanambú, Corresponsal [Regional newspaper repository of Centro Cultural Leopoldo López Álvarez del Banco de la República en Pasto, Nariño, Colombia]: *El Derecho*, 20 August 1936.
- El Derecho, 1936e, Se teme una nueva catástrofe producida por el volcán Doña Juana. Donde se han producido derrumbes de leguas de extensión, Corresponsal [Regional newspaper repository of Centro Cultural Leopoldo López Álvarez del Banco de la República en Pasto, Nariño, Colombia]: *El Derecho*, 22 August 1936.
- El Derecho, 1936f, Los terremotos del Sur, Corresponsal [Regional newspaper repository of Centro Cultural Leopoldo López Álvarez del Banco de la República en Pasto, Nariño, Colombia]: *El Derecho* local newspaper, 11 December 1936.
- El Heraldo, 1899, El volcán Doña Juana, Corresponsal [National newspaper repository at the library Luis Angel Arango, Bogotá]: *El Heraldo*, 4 February 1899.
- El Tiempo, 1936, Una erupción del volcán ‘Doña Juana’ causó grandes estragos, Corresponsal, El Tiempo [National newspaper repository at the library Luis Angel Arango, Bogotá]: *El Tiempo*, 15 August 1936.
- Espinosa, A., 2012, *Enciclopedia de Desastres Naturales Históricas en Colombia* (2nd ed.): Pereira, Colombia, Academia Colombiana de Ciencias Exactas, Físicas y Naturales, Universidad del Quindío, 1840 p.
- Espinosa-Arango, M.L., and Prieto, D., 2022, Entre el tiempo de páramo y la atmósfera del posconflicto en Colombia: Una antropología de la vida en el volcán-páramo Doña Juana, in Dabezies, J.M., and Arregui, A.G., eds., *Vitalidades: Etnografías en los límites de lo Humano: Madrid, Spain, Nola editores*, 278 p.
- ESRI, 2019, ArcGIS for Desktop: Release 10.3: Redlands, California, Environmental Systems Research Institute.

- Fisher, R.V., and Heiken, G., 1982, Mt. Pelée, Martinique: May 8 and 20, 1902, pyroclastic flows and surges: *Journal of Volcanology and Geothermal Research*, v. 13, p. 339–371, [https://doi.org/10.1016/0377-0273\(82\)90056-7](https://doi.org/10.1016/0377-0273(82)90056-7).
- Fisher, R.V., and Schmincke, J.-U., 1984, *Pyroclastic Rocks*: Berlin, Springer-Verlag, 472 p., <https://doi.org/10.1007/978-3-642-74864-6>.
- Formenti, Y., Druitt, T.H., and Kelfoun, K., 2003, Characterisation of the 1997 Vulcanian explosions of Soufrière Hills volcano, Montserrat, by video analysis: *Bulletin of Volcanology*, v. 65, p. 587–605, <https://doi.org/10.1007/s00445-003-0288-8>.
- Freundt, 1999, Formation of high-grade ignimbrites: Part II. A pyroclastic suspension current model with implications also for low-grade ignimbrites: *Bulletin of Volcanology*, v. 60, p. 545–567, <https://doi.org/10.1007/s004450050251>.
- Giordano, G., and Cas, R.A.F., 2021, Classification of ignimbrites and their eruptions: *Earth-Science Reviews*, v. 220, <https://doi.org/10.1016/j.earscirev.2021.103697>.
- Gómez-Bolaños, A.F., 2012, Belén Nariño: Memorias del Pasado [unedited undergraduate thesis]: Pasto, Colombia, Department of Social Sciences, Universidad de Nariño, 112 p.
- Gottsmann, J., De Angelis, S., Fournier, N., Van Camp, M., Sacks, S., Linde, A., and Ripepe, M., 2011, On the geophysical fingerprint of Vulcanian explosions: *Earth and Planetary Science Letters*, v. 306, p. 98–104, <https://doi.org/10.1016/j.epsl.2011.03.035>.
- Gregory-Wodzicki, K.M., 2000, Uplift history of the Central and Northern Andes: A review: *Geological Society of America Bulletin*, v. 112, no. 7, p. 1091–1105, [https://doi.org/10.1130/0016-7606\(2000\)112<1091:UHOT-CA>2.0.CO;2](https://doi.org/10.1130/0016-7606(2000)112<1091:UHOT-CA>2.0.CO;2).
- Hayashi, J.N., and Self, S., 1992, A comparison of pyroclastic flow and debris avalanche mobility: *Journal of Geophysical Research*, v. 97, p. 9063–9071, <https://doi.org/10.1029/92JB001173>.
- Hidalgo, S., Monzier, M., Almeida, E., Chazot, G., Eissen, J.P., van der Plicht, J., and Hall, M.L., 2008, Late Pleistocene and Holocene activity of Atacazo–Ninahuilca volcanic complex (Ecuador): *Journal of Volcanology and Geothermal Research*, v. 176, p. 16–26, <https://doi.org/10.1016/j.jvolgeores.2008.05.017>.
- Iverson, R.M., 1997, The physics of debris flows: *Reviews of Geophysics*, v. 35, p. 245–296, <https://doi.org/10.1029/97RG00426>.
- Jenkins, S.F., Magill, C.R., and McAneney, K.J., 2007, Multi-stage volcanic events: A statistical investigation: *Journal of Volcanology and Geothermal Research*, v. 161, p. 275–288, <https://doi.org/10.1016/j.jvolgeores.2006.12.005>.
- Jenkins, S.F., Phua, M., Warren, J.F., Biass, S., and Bouvet de Maisonneuve, C., 2020, Reconstructing eruptions from historical accounts: Makaturing c. 1765, Philippines: *Journal of Volcanology and Geothermal Research*, v. 404, <https://doi.org/10.1016/j.jvolgeores.2020.107022>.
- Küch, R., 1892, Petrographie I. Die vulkanischen Gesteine, in Reiss, W., and Stübel, A., eds., *Reisen in Süd Amerika*, Geologische Studien in der Republik Colombia: Berlin, Germany, I.A. Asher Verlag, 308 p.
- Le Pennec, J.L., Ruiz, A.G., Eissen, J.P., Hall, M.L., and Fornari, M., 2011, Identifying potentially active volcanoes in the Andes: Radiometric evidence for late Pleistocene–early Holocene eruptions at Volcán Imbabura, Ecuador: *Journal of Volcanology and Geothermal Research*, v. 206, p. 121–135, <https://doi.org/10.1016/j.jvolgeores.2011.06.002>.
- Lerner, G.A., Cronin, S.J., Bebbington, M.S., and Platz, T., 2019, The characteristics of a multi-episode volcanic regime: The post-AD 960 Maero eruptive period of Mt. Taranaki (New Zealand): *Bulletin of Volcanology*, v. 81, p. 61, <https://doi.org/10.1007/s00445-019-1327-4>.
- Le Roux, J.P., 2003, Can dispersive pressure cause inverse grading in grain flows?: Discussion: *Journal of Sedimentary Research*, v. 73, p. 333–334, <https://doi.org/10.1306/043002730333>.
- Lucchi, F., 2013, Stratigraphic methodology for the geological mapping of volcanic areas: insights from the Aeolian archipelago (southern Italy), in Lucchi, F., Peccerillo, A., Keller, J., Tranne, C.A., and Rossi, P.L., eds., *The Aeolian Islands Volcanoes: Geological Society*, London, Memoir 37, p. 37–53, <https://doi.org/10.1144/M37.5>.
- Lucchi, F., Sulpizio, R., Meschiari, S., Tranne, C.A., Albert, P.G., Mele, D., and Dellino, P., 2022, Sedimentological analysis of ash-rich pyroclastic density currents, with special emphasis on syn-depositional erosion and clast incorporation: The Brown Tuff eruptions (Vulcano, Italy): *Sedimentary Geology*, v. 427, <https://doi.org/10.1016/j.sedgeo.2021.106040>.
- Macías, J.L., Arce, J.L., García-Tenorio, F., Sosa-Ceballos, G., and Gardner, J.E., 2020, Source and behavior of pyroclastic density currents generated by Vulcanian-style explosions of Popocatepetl volcano (Mexico) on 22 January 2001: *Journal of Volcanology and Geothermal Research*, v. 406, <https://doi.org/10.1016/j.jvolgeores.2020.107071>.
- Macorps, E., Carbonnier, S.J., Varley, N.R., Capra, L., Atlas, Z., and Cabré, J., 2018, Stratigraphy, sedimentology and inferred flow dynamics from the July 2015 block-and-ash flow deposits at Volcán de Colima, Mexico: *Journal of Volcanology and Geothermal Research*, v. 349, p. 99–116, <https://doi.org/10.1016/j.jvolgeores.2017.09.025>.
- Massaro, S., Costa, A., Sulpizio, R., Coppola, D., and Capra, L., 2019, Cyclic activity of the Fuego de Colima volcano (Mexico): Insights from satellite thermal data and nonlinear models: *Solid Earth*, v. 10, p. 1429–1450, <https://doi.org/10.5194/se-10-1429-2019>.
- Miyabuchi, Y., 1999, Deposits associated with the 1990–1995 eruption of Unzen volcano, Japan: *Journal of Volcanology and Geothermal Research*, v. 89, p. 139–158, [https://doi.org/10.1016/S0377-0273\(98\)00129-2](https://doi.org/10.1016/S0377-0273(98)00129-2).
- Monsalve-Bustamante, M.L., 2020, The volcanic front in Colombia: Segmentation, recent and historical activity, in Gómez, J., and Pinilla-Pachon, A.O., eds., *The Geology of Colombia, Volume 4—Quaternary*: Servicio Geológico Colombiano Publicaciones Geológicas Especiales 38, p. 97–159.
- Monteil, C., Barclay, J., and Hicks, A., 2020, Remembering, forgetting, and absencing disasters in the post-disaster recovery process: *International Journal of Disaster Risk Science*, v. 11, p. 287–299, <https://doi.org/10.1007/s13753-020-00277-8>.
- Montgomery, D.R., Balco, G., and Willet, S.D., 2001, Climate, tectonics, and the morphology of the Andes: *Geology*, v. 29, no. 7, p. 579–582, [https://doi.org/10.1130/0091-7613\(2001\)029<0579:CTATMO>2.0.CO;2](https://doi.org/10.1130/0091-7613(2001)029<0579:CTATMO>2.0.CO;2).
- Mora, A., Parra, M., Strecker, M., Sobel, E.R., Hooghiemstra, H., and Torres, V., 2008, Climatic forcing of asymmetric orogenic evolution in the Eastern Cordillera of Colombia: *Geological Society of America Bulletin*, v. 120, no. 7–8, p. 930–949, <https://doi.org/10.1130/B26186.1>.
- Nakada, S., and Fujii, T., 1993, Preliminary report on the activity at Unzen Volcano (Japan), November 1990–November 1991: Dacite lava domes and pyroclastic flows: *Journal of Volcanology and Geothermal Research*, v. 54, no. 3–4, p. 319–333, [https://doi.org/10.1016/0377-0273\(93\)90070-8](https://doi.org/10.1016/0377-0273(93)90070-8).
- Pardo, N., Pulgarín, B., Betancourt, V., Lucchi, F., and Valencia, L.J., 2019, Facing geological mapping at low-latitude volcanoes: The Doña Juana volcanic complex study-case, SW Colombia: *Journal of Volcanology and Geothermal Research*, v. 385, p. 46–67, <https://doi.org/10.1016/j.jvolgeores.2018.04.016>.
- Pensa, A., Capra, L., Giordano, G., and Corrado, S., 2018, Emplacement temperature estimation of the 2015 dome collapse of Volcán de Colima as key proxy for flow dynamics of confined and unconfined pyroclastic density currents: *Journal of Volcanology and Geothermal Research*, v. 357, p. 321–338, <https://doi.org/10.1016/j.jvolgeores.2018.05.010>.
- Pereira-Gamba, F., 1919, *La Vida de los Andes Colombianos*: Quito, Ecuador, El Progreso, 233 p., <http://www.banrepcultural.org/blaavirtual/modosycostumbres/andcol/index.htm>.
- Platz, T., Cronin, S.J., Cashman, K.V., Stewart, R.B., and Smith, I.E.M., 2007, Transition from effusive to explosive phases in andesite eruptions—A case-study from the AD 1655 eruption of Mt. Taranaki, New Zealand: *Journal of Volcanology and Geothermal Research*, v. 161, p. 15–34, <https://doi.org/10.1016/j.jvolgeores.2006.11.005>.
- Platz, T., Cronin, S.J., Procter, J.N., Neall, V.E., and Foley, S.F., 2012, Non-explosive, dome-forming eruptions at Mt. Taranaki, New Zealand: *Geomorphology*, v. 136, p. 15–30, <https://doi.org/10.1016/j.geomorph.2011.06.016>.
- Reimer, P.J., et al., 2020, The IntCal20 Northern Hemisphere radiocarbon age calibration curves (0–55 cal kBP): *Radiocarbon*, v. 62, no. 4, p. 725–757, <https://doi.org/10.1017/RDC.2020.41>.
- Robin, C., Samaniego, P., Le Pennec, J.L., Mothes, P., and van der Plicht, J., 2008, Late Holocene cycles of dome growth and Plinian activity at Guagua Pichincha volcano (Ecuador): *Journal of Volcanology and Geothermal Research*, v. 176, p. 7–15, <https://doi.org/10.1016/j.jvolgeores.2007.10.008>.
- Robin, C., Samaniego, P., Le Pennec, J.L., Fornari, M., Mothes, P., and van der Plicht, J., 2010, New radiometric and petrological constraints on the evolution of the Pichincha volcanic complex (Ecuador): *Bulletin of Volcanology*, v. 72, p. 1109–1129, <https://doi.org/10.1007/s00445-010-0389-0>.
- Samaniego, P., Monzier, M., Robin, C., and Hall, M.L., 1998, Late Holocene eruptive activity at Nevado Cayambe volcano, Ecuador: *Bulletin of Volcanology*, v. 59, p. 451–459, <https://doi.org/10.1007/s004450050203>.
- Savage, S.B., and Lun, C.K.K., 1988, Particle size segregation in inclined chute flow of dry cohesionless granular solids: *Journal of Fluid Mechanics*, v. 189, p. 311–335, <https://doi.org/10.1017/S0022121208800103X>.
- Schwarzkopf, L.M., Schmincke, H.U., and Cronin, S.J., 2005, A conceptual model for block-and-ash flow basal avalanche transport and deposition, based on deposit architecture of 1998 and 1994 Merapi flows: *Journal of Volcanology and Geothermal Research*, v. 139, p. 117–134, <https://doi.org/10.1016/j.jvolgeores.2004.06.012>.
- Servicio Geológico Colombiano, 2022, *Volcanes de Colombia*: <https://www.sgc.gov.co/volcanes>.
- Siddiqi, A., Peters, K., and Zulver, J., 2019, ‘Doble afectación’: Living with disasters and conflict in Colombia: London, UK, ODI, <https://odi.org/en/publications/doble-afectacion-living-with-disasters-and-conflict-in-colombia/> (accessed 15 October 2022).
- Stinton, A.J., Cole, P.D., Stewart, R.C., Odbert, H.M., and Smith, P., 2014, The 11 February 2010 partial dome collapse at Soufrière Hills volcano, Montserrat, in Wadge, G., Robertson, R.E.A., and Voight, B., eds., *The Eruption of Soufrière Hills Volcano, Montserrat from 2000 to 2010*: Geological Society, London, Memoir 39, p. 133–152, <https://doi.org/10.1144/M39.7>.
- Sulpizio, R., and Dellino, P., 2008, Sedimentology, depositional mechanisms and pulsating behavior of pyroclastic density currents, in Gottsmann, J., and Martí, J., eds., *Developments in volcanology, Calderas Volcanism: Analysis, Modelling and Response*: Amsterdam, Netherlands, Elsevier, v. 10, p. 57–96, [https://doi.org/10.1016/S1871-644X\(07\)00002-2](https://doi.org/10.1016/S1871-644X(07)00002-2).
- Sulpizio, R., Mele, D., Dellino, P., and La Volpe, L., 2007, Deposits and physical properties of pyroclastic density currents during complex subplinian eruptions: The AD 472 (Pollena) eruption of Somma-Vesuvius, Italy: *Sedimentology*, v. 54, p. 607–635, <https://doi.org/10.1111/j.1365-3091.2006.00852.x>.
- Sulpizio, R., Capra, L., Sarocchi, D., Saucedo, R., Gavilanes-Ruiz, J.C., and Varley, N.R., 2010, Predicting the block-and-ash flow inundation areas at Volcán de Colima (Colima, México) based on the present day (February 2010) status: *Journal of Volcanology and Geothermal Research*, v. 193, p. 49–66, <https://doi.org/10.1016/j.jvolgeores.2010.03.007>.
- Sulpizio, R., Dellino, P., Doronzo, D.M., and Sarocchi, D., 2014, Pyroclastic density currents—State of the art and perspectives: *Journal of Volcanology and Geothermal Research*, v. 283, p. 36–65, <https://doi.org/10.1016/j.jvolgeores.2014.06.014>.
- Taboada, A., Rivera, L.A., Fuenzalida, A., Cisternas, A., Philip, H., Bijwaard, H., Olaya, J., and Rivera, C., 2000, Geodynamics of the northern Andes: Subduction

- and intracontinental deformation (Colombia): *Tectonics*, v. 19, p. 787–813, <https://doi.org/10.1029/2000TC900004>.
- Voight, B., 1990, The 1985 Nevado del Ruiz volcano catastrophe: Anatomy and retrospection: *Journal of Volcanology and Geothermal Research*, v. 44, no. 3–4, p. 349–386, [https://doi.org/10.1016/0377-0273\(90\)90027-D](https://doi.org/10.1016/0377-0273(90)90027-D).
- Walker, G.P.L., Wilson, L., and Bowell, E.L.G., 1971, Explosive volcanic eruptions I: The rate of fall of pyroclasts: *Geophysical Journal of the Royal Astronomical Society*, v. 22, p. 377–383, <https://doi.org/10.1111/j.1365-246X.1971.tb03607.x>.
- Walker, R.G., 1983, Cardium Formation 3. Sedimentology and stratigraphy in the Garrington-Caroline area, Alberta: *Bulletin of Canadian Petroleum Geology*, v. 31, no. 4, p. 213–230, <https://doi.org/10.35767/gscpgbull.31.4.213>.
- Watts, R.B., 2002, Growth patterns and emplacement of the andesitic lava dome at Soufrière Hills volcano, Montserrat, *in* Druitt, T.H., and Kokelaar, B.P., eds., *The Eruption of Soufrière Hills Volcano, Montserrat*, from 1995 to 1999: Geological Society, London, *Memoir* 21, p. 115–152, <https://doi.org/10.1144/GSL.MEM.2002.021.01.06>.

SCIENCE EDITOR: BRAD SINGER
ASSOCIATE EDITOR: MICHAEL ORT

MANUSCRIPT RECEIVED 21 APRIL 2022
REVISED MANUSCRIPT RECEIVED 3 SEPTEMBER 2022
MANUSCRIPT ACCEPTED 15 OCTOBER 2022

Printed in the USA